Spaceborne Lidar in the Study of Marine Systems

Authors

Chris Hostetler, NASA Langley Research Center, Hampton, Virginia 23681-2199; email: chris.a.hostetler@nasa.gov (corresponding author)

Michael J. Behrenfeld, Department of Botany and Plant Pathology, Oregon State University, Corvallis, Oregon, 97331-2902; email: mjb@science.oregonstate.edu

Yongxiang Hu, NASA Langley Research Center, Hampton, Virginia 23681-2199; email: yongxiang.hu-1@nasa.gov

Johnathan W. Hair, NASA Langley Research Center, Hampton, Virginia 23681-2199; email: johnathan.w.hair@nasa.gov

Jennifer A. Schulien, Department of Botany and Plant Pathology, Oregon State University, Corvallis, Oregon, 97331-2902; email: schuliej@oregonstate.edu

Keywords

Lidar, remote sensing, ocean plankton, atmospheric corrections, aerosols, clouds

Abstract

Satellite passive ocean color instruments have provided an unbroken ~20-year record of global ocean plankton properties, but this measurement approach has inherent limitations in terms of spatial-temporal sampling and ability to resolve vertical structure within the water column. These limitations can be addressed by coupling ocean color data with measurements from a spaceborne lidar. Airborne lidars have been used for decades to study ocean subsurface properties, but recent breakthroughs have now demonstrated that plankton properties can be measured with a satellite lidar. The satellite lidar era in oceanography has arrived. Here we present a review of the lidar technique, its applications in marine systems, a prospective on what can be accomplished in the near future with an ocean- and atmosphere-optimized satellite lidar, and a vision for a multi-platform 'virtual constellation' of observational assets enabling a 3-dimensional reconstruction of global ocean ecosystems.

Table of Contents

1. INTRODUCTION

Marine ecosystems are complex entities encompassing vast numbers of species functioning over a wide range of spatial and temporal scales. Phytoplankton constitute the base of most marine ecosystems and their annual net photosynthetic carbon fixation is roughly equivalent to that of all terrestrial plants (Field et al. 1998; Behrenfeld et al. 2001). This production at the base of the aquatic food chain drives CO_2 exchange between the atmosphere and ocean and fuels carbon sequestration to the deep sea (Falkowski et al. 1998; DeVries et al. 2012). Accordingly, plankton productivity plays a vital role in Earth's coupled ocean-atmosphere system. Furthermore, and in stark contrast to terrestrial vegetation, the entire global ocean phytoplankton stock is consumed and regrown every week (Antoine et al. 1996; Behrenfeld & Falkowski 1997). This rapid turnover underpins ocean food webs and, hence, fish stocks and global food supply. In addition, and through an array of trophic interactions and metabolisms, some of the organic carbon products initially produced by phytoplankton become converted into volatilized molecules that leave the surface ocean and function as important atmospheric aerosols that influence clouds and the Earth's radiative budget (Falkowski et al. 1992; Gantt & Meskhidze 2013; Meskhidze & Nenes 2006).

Our understanding of links between biodiversity, ecosystem structure, and ecological and biogeochemical function is incomplete, as is our grasp of how these linkages and processes vary over space and time. With our current observational and modeling tools, we have only begun to constrain the flow and cycling of elements within and between ecosystems or the impact of climate and other physical and chemical environmental changes on ecological systems. However, from this work, clear paths have emerged for accelerating our understanding. Global satellite ocean observations are fundamental to these future scientific breakthroughs.

Many scientific advances have been made using satellite passive ocean color data (McClain 2009), but there are fundamental geophysical properties that simply cannot be characterized with

this technology alone (Section 2). The historical single-sensor (i.e., ocean color) approach for global ocean biology and biogeochemistry research contrasts sharply with the multi-instrument strategies used for atmospheric research. The A-Train constellation (ref A-Train) ushered in a new era of remote sensing wherein synergies between data sets acquired by multiple instruments were routinely exploited to advance science. This includes the application of data sets from different types of sensors to draw conclusions on various processes, the use of data from one or more sensors to assess and improve algorithms for another sensor, and the use of data from two or more sensors in joint algorithms to provide new or improved data products. For instance, the CCCM radiative flux data product (Kato et al. 2011) combines active and passive measurements from four instruments[1] on three satellites to provide the vertical distribution of cloud and aerosol properties and profiles of radiative flux to much greater accuracy than possible using any one sensor alone. Following such examples, two instruments are being considered for the Plankton Aerosol Cloud and marine Ecosystem (PACE) mission, a hyperspectral ocean color sensor and a co-deployed polarimeter. Here, the polarimeter complements the ocean color sensor by enabling more accurate atmospheric corrections, as well as potential ocean retrievals of particle type (Loisel et al. 2008). While this two-instrument PACE complement offers significant advantages, even greater synergies can be achieved by the combination of passive ocean color with an ocean-optimized profiling lidar.

In this paper, we briefly review strengths and limitations of passive ocean color measurements (Section 2), present ocean lidar fundamentals (Section 3), describe airborne lidar measurements of ocean properties (Section 4), overview the current state of spaceborne lidar ocean remote sensing

[1] CCCM stands for CERES CALIPSO Cloudsat MODIS. The CCCM algorithms employ data from the CERES broadband radiometer and MODIS spectroradiometer on the Aqua satellite, the CALIOP lidar on the CALIPSO satellite (see Sections 3 and 5), the Cloud Profiling Radar on the CloudSat satellite.

(Section 5), introduce an ocean-optimized lidar concept achievable in the near term with interdisciplinary science applications (Sections 6 & 7), and introduce a multi-platform vision of synergistic space and field observations for global biogeochemical and ecosystem research (Section 8).

2. PASSIVE OCEAN COLOR: ADVANCES AND CHALLENGES

In the modern era of Earth System science, the availability of global satellite-based observations is all too easily taken for granted. Yet, for the oceanographic community, such data are still a relatively new development, with the continuous global data record extending back less than 20 years. The Sea-viewing Wide Field of View Sensor (SeaWiFS) was the first ocean color sensor to provide multi-year, fully global ocean color data. The SeaWiFS design was built upon the proof-of-concept Coastal Zone Color Scanner (CZCS) and provided measurements at 8 spectral bands originally targeting a modest set of ocean geophysical properties (e.g., chlorophyll concentration). Subsequent missions (e.g., MODIS, MERIS, VIIRS) largely continued these heritage measurements, with some expansion (e.g., chlorophyll fluorescence bands on MODIS and MERIS) and improved spatial resolution and signal-to-noise. The science community, on the other hand, has greatly expanded the suite of retrieved ocean properties beyond the original targets.

Today, passive ocean color data are used to quantify surface layer chlorophyll concentrations, total particulate carbon stocks, and net primary production (McClain 2009). The development and application of spectral inversion algorithms (Garver & Siegel 1997; Maritorena et al. 2002; Lee et al. 2002; Werdell et al. 2013) to ocean color data has further provided assessments of absorption by colored dissolved organic matter, phytoplankton absorption coefficients, total particulate backscatter coefficients (Lee et al. 2002; Maritorena et al. 2002, Siegel et al. 2002, 2005; Werdell et al. 2013), and estimates of phytoplankton carbon biomass and division rates (Behrenfeld et al.

2005; Westberry et al. 2008; Silsbe et al. 2016). The combination of fluorescence line height data and phytoplankton pigment and carbon data has yielded insights on iron stress and photophysiology (Behrenfeld et al. 2009; Westberry et al. 2013; Lin et al. 2016). Additional algorithm development has led to new retrievals regarding plankton community composition, including phytoplankton size fractions, slope of the particle size distribution, and even specific phytoplankton groups, such as coccolithophores, *Trichodesimum*, and harmful algal species (e.g., Alvain et al. 2005; Bracher et al. 2009; Sadeghi et al. 2012; Kostadinov et al 2010; IOCCG 2014 and references therein). Furthermore, the sustained time series of these diverse ocean properties has provided major advances in our understanding of plankton annual cycles and responses to climate variations and has been instrumental for informing and testing ocean ecosystem models. Quite simply, the satellite ocean color record has fostered a major revolution in oceanography, one we can hope will continue with upcoming advanced sensors such as the hyperspectral instrument planned for the PACE mission.

Despite the major advances enabled through ocean color observations, the passive radiometric technique has several fundamental limitations. Specifically, (1) the top-of-atmosphere signal measured by the sensors includes contributions from sources other than the target ocean properties, (2) the ocean color signal provides no information on the vertical distribution of ocean constituents, (3) measured ocean color is an optically integrated property without a direct signal for separating the absorption and scattering fractions, and (4) global sampling is compromised by atmospheric interferences and solar angle.

With respect to the first limitation, there can be large uncertainties in retrieved parameters due to uncertainty in corrections for scattering and absorption from sources other than water molecules and particles suspended in seawater. The radiances measured by ocean color instruments are

composed of several terms: scattered sunlight from ocean subsurface particles and water molecules, subsurface bubbles, surface foam, the surface interface itself, and atmospheric constituents, including aerosols, clouds, and air molecules. Easily 90% of the top-of-atmosphere measured signal can be due to scattering from the atmosphere. A small error in the estimation and removal of this atmospheric contribution creates a large relative error in the estimated water leaving radiances and associated geophysical retrievals. Similarly, unaccounted for contributions from bubbles, foam, and surface reflection degrade retrieval fidelity. Under particularly challenging conditions (e.g., sunglint, significant aerosol loads, nearby clouds), attempts to retrieve ocean properties are abandoned all together.

With respect to the second ocean color limitation, the ocean color signal is heavily weighted toward the surface. This results from the exponential decay of sunlight with depth due to absorption from water, particles, and dissolved matter. Similarly, the up-scattered photons suffer the same exponential decay on their path to the ocean surface. The result is that over 92% of the ocean color signal emanates from the first optical depth (10 m geometric depth if the diffuse attenuation coefficient = 0.1 m^{-1}) and 71% the first half of the first optical depth (5 m for the same case). This limitation of ocean color can result in significant errors in important water-column-integrated ocean properties, such as chlorophyll concentration (Stramska & Stramski 2005; Sathyendranath & Platt 1989) or net primary production (NPP) (Platt & Sathyendranath 1988, Churnside 2015; Jacox et al. 2015).

With respect to the third ocean color limitation, the strength and spectral characteristics of retrieved water leaving radiances represent the integrated signature of multiple factors. Dominant contributors to the signal include absorption by colored dissolved matter (a_{cdm}), phytoplankton pigments (a_{ph}), and non-algal particles (a_{nap}), plus backscattering by suspended particles (b_{bp})

(note, the absorption and scattering by saltwater is a known function of salinity). Retrievals of these four fundamental properties and other geophysical parameters derived from them have an inherent uncertainty that cannot be reduced without additional information. This issue is a driving motivation for the PACE mission's expanded measurement spectral range and resolution compared to heritage ocean color missions. Coupling such passive ocean color measurements with active satellite instruments can likewise reduce uncertainties in derived ocean properties.

Finally, with respect to the fourth limitation, ocean color global sampling is significantly limited by atmospheric interferences and sun angle. On average, greater than 70% of the Earth's ocean area is under sufficient cloud cover to make passive ocean retrievals impossible. Broken cloud scenes are a significant fraction of the remaining ocean area and, under these conditions, side-scatter from nearby clouds can compromise accurate ocean retrievals from otherwise clear sky pixels. Beyond issues of cloudiness, ocean color retrievals must be abandoned when strongly scattering aerosol layers are present. Some of these aerosol interferences can compromise ocean color monitoring for extended periods. Examples of such conditions include pollution outflow from populated regions (e.g., Eastern Seaboard of the US, India, China), systematic dust events (e.g., Saharan dust outflow at low northern latitudes in the Atlantic, Gobi dust outflow at mid latitudes in the Northern Pacific), and long-range and broadly distributed smoke transport (e.g., from boreal forest fires in North America and Siberia, agricultural fires from all continents). In polar regions, low sun angles, by themselves and exacerbated by cloud conditions (i.e., cloud shadowing of otherwise clear pixels), can eliminate ocean color sampling from late fall through early spring. Notably, these high latitude regions include some of the most productive waters in the global oceans and the lack of sampling for a significant fraction of the year can undermine any complete understanding of plankton annual cycles and biogeochemistry (Behrenfeld et al. 2017).

The intent of this section is not to criticize the passive ocean color approach, but rather to recognize both its benefits and inherent weaknesses and thereby highlight where additional technologies may contribute to improved understanding of global ocean ecosystems. Passive ocean color radiometry has enabled huge scientific advances and will remain a cornerstone of future ocean research. With increases in spectral coverage and resolution from missions like PACE and work toward increasing the number and coverage of geostationary sensors, such as Geostationary Ocean Color Imager (GOCI) (Ryu et al. 2012; O'Malley et al. 2014), the ocean color portfolio is set to expand significantly. With these new ocean color capabilities on the horizon, it is time to consider complementary remote sensing techniques that will enable additional breakthrough science on issues beyond the reach of passive radiometry. Lidar is just such a technique that, when flown in formation with a capable ocean color sensor, can revolutionize satellite ocean remote sensing.

3. LIDAR 101

Airborne lidars have been used for decades to study the atmosphere and the oceans. However, a longstanding question has been whether lidars can achieve the sensitivity required to provide useful ocean products from space. That question was answered decisively with data from the Cloud-Aerosol Lidar with Orthogonal Polarization (CALIOP) instrument that has operated in space since 2006 on the Cloud-Aerosol Lidar and Infrared Pathfinder Satellite Observation (CALIPSO) platform (Winker et al. 2009). While CALIOP was designed solely for atmospheric measurements and has severe drawbacks as an ocean lidar, Yongxiang Hu developed an innovative technique for retrieving ocean subsurface particulate backscatter from CALIOP data (Hu 2009). But before telling the story of ocean science breakthroughs made with CALIOP, we here provide some background explanation of the lidar technique.

Lidar is an acronym for light detection and ranging. Similar to radar, a lidar employs a time-of-flight technique to provide range-resolved (i.e., for the current discussion, 'vertically-resolved') measurements of optical properties. Unlike the ocean color technique's reliance on the sun as a source of light (thus, 'passive' remote sensing), a lidar uses lasers to generate its own photons that are ultimately scattered back to the instrument's receiver (thus, 'active' remote sensing). **Figure 1** provides a simple illustration of the lidar approach, where the geometry depicted is a nadir or near-nadir viewing configuration. In this figure, laser pulses are directed downward and a small fraction of the backscattered light is collected in a telescope receiver. In the atmosphere, this backscattered light originates from air molecules and suspended particles, such as cloud droplets or aerosol particles. Similarly, the laser pulse is backscattered in the ocean by water molecules and suspended particles, such as phytoplankton. These signals are received by the telescope and imaged onto a high-speed optical detector. This detector generates a time-varying electrical signal that is proportional to the instantaneous optical power incident on the detector, and this electrical signal is recorded at a high sampling rate (e.g., 10^7 to 10^8 samples/s). The point of origin of the signal (in other words its vertical position in the atmosphere or ocean) is determined using the speed of light. Specifically, each sample is assigned a distance from the lidar based on the time difference between the firing of the laser and the detection of the backscattered signal. By sequentially recording all of the samples following a laser pulse into a data array, a vertically-resolved profile is created, with each sample reflecting the magnitude of scattering at a known altitude in the atmosphere or depth into the ocean (**Figure 1d)**. Importantly, the vertical resolution of a lidar profile is determined by the rate of sampling by its detector. For example, a rate of 10^7 samples/s corresponds to the 15 m vertical resolution commonly used for atmospheric

measurements, whereas a rate of 10^8 samples/s would correspond to a ~1 m vertical resolution that is more appropriate for ocean profiling.

For the scenario described above, a vertical profile of the atmosphere and ocean is acquired for every laser pulse. Combining data from multiple laser pulses thus creates a time series of profiles. When a lidar is mounted on a moving platform, such as an aircraft or satellite, this time series maps to a horizontally and vertically resolved data 'curtain' registered to the flight track (an example is shown in **Section 4**). One advantage of active lidar remote sensing is that it creates these 'curtains' of data during both day and night, thus providing opportunities to study diel changes in plankton properties and to continue observations during periods of polar night. During daylight hours, the contribution to the received signal from diffusely scattered sunlight is estimated from data acquired between laser pulses and subtracted from the measured profiles.

Producing useful geophysical data products from the measured lidar signals requires application of appropriate calibration factors and post-processing algorithms. Perhaps more importantly, the suite of products that can be produced and their accuracy depend on instrument design (e.g., the number and character of the receiver channels). Our illustration and discussion to this point has centered on the 'elastic backscatter lidar' technique, which relies on backscatter from air molecules and particles at the same wavelength as the transmitted laser pulse. Many atmosphere-ocean lidars employ alternate techniques involving additional optical processing in the receiver downstream of the telescope to expand retrieval capabilities. An important example of this is the separation of polarization and spectral components of the received signal onto different detectors. By doing so, simultaneous profiles sensitive to different physical properties are measured on each detector, thereby increasing information content in the measurements and expanding the number and accuracy of retrieved products. Lidars capable of generating an array

of geophysical data products have been demonstrated for decades from stationary platforms, ships, and aircraft. Scientific progress made with airborne lidars motivates some of our thinking about a future ocean-optimized satellite lidar and we focus on three airborne applications in the next section.

4. ESSAYS FROM THE FIELD

The first scientifically meaningful oceanographic applications of airborne lidar involved the use of fluorescence techniques, starting with chlorophyll (Kim et al. 1973) and later colored dissolved organic matter (CDOM) (Hoge et al. 1995). Fluorescence involves absorption of a photon of light by a constituent molecule and subsequent emission of a photon as that molecule relaxes back to a lower energy state. Chlorophyll readily absorbs the common 532 nm laser wavelength employed in many lidars and emits fluorescence in the 670-690 nm region. Detecting the signal alone does not provide a useful measurement, however. One must correct the magnitude of signal for factors that are unrelated to chlorophyll concentration, such as variations in laser energy, atmospheric attenuation, and water attenuation. These corrections were made by dividing the measured fluorescence by Raman-shifted backscatter from water molecules[2] measured at a different wavelength (Bristow et al. 1981) under the assumption that the aforementioned factors unrelated to chlorophyll cancel in the ratio (Poole & Esais 1982). The result is a relative, rather than absolute, measure of chlorophyll fluorescence. The ocean lidar research group at NASA Wallops Flight Facility made the most significant scientific contributions in this field with their Airborne Oceanographic Lidar (AOL) (Hoge et al. 1981). That lidar employed a grating spectrometer in the receiver to isolate the chlorophyll fluorescence and Raman-shifted water

[2] The O-H vibrational stretching mode of the water molecule causes a frequency shift for a fraction of the scattered photons by 3418 cm-1. For 532 nm laser excitation, the Raman-shifted water backscatter is at 645 nm.

backscatter. This water-Raman-normalized chlorophyll fluorescence signal was used in many studies. For instance, Yoder et al. (1993) used chlorophyll fluorescence signals acquired with the AOL during flights on a long-range P3-B aircraft to study spatial scales of the North Atlantic bloom. From these measurements, they concluded that the pixel resolution of CZCS, SeaWiFS, and MODIS ocean color data captured the dominant scales of variability in the bloom and that mesoscale variability must be taken into account in the interpretation of ship-based measurements to avoid confusing changes due to advection with those due to local ecosystem processes. Martin et al. (1994) used data from AOL during the IronEx in situ enrichment experiment to test the hypothesis that iron is a limiting factor for phytoplankton productivity in the equatorial Pacific. AOL fluorescence data were further used by Hoge et al. (2003) to validate MODIS ocean color fluorescence line height products. Hoge et al. (2005) subsequently used both AOL chlorophyll and CDOM fluorescence measurements to quantify chlorophyll biomass, using a modification of an ocean color algorithm and matchup data with ship-based in situ measurements to appropriately scale their fluorescence-to-Raman ratios.

Due to weak signal levels, fluorescence retrievals typically involved vertically integrating the received backscatter to provide a column-wise value rather than a series of profiles along the flight track. True profiling measurements were first made possible with the application of the elastic backscatter lidar technique described in Section 3. Airborne implementations of this technique were demonstrated in the late 1900s by groups from around the world, including those from Australia (Billard et al. 1986), the US (e.g., Hoge et al. 1988; Smart & Kwon 1996), and Russia (Bunkin & Surovegin 1992). A major challenge to this technique is ambiguity in the interpretation of the measured signal. The variation of the measured signal with depth depends on several known parameters (e.g., range and molecular density) and two unknowns: the coefficients of particulate

backscatter and attenuation. Retrieving one of the unknowns requires assumptions on the behavior of the other, and such assumptions are uncertain and not universally valid. Another fundamental problem is that the measurement is difficult to calibrate. Because of these two issues, early results were typically confined to relative, rather than absolute, estimates of particulate backscatter and approximate estimates of the attenuation coefficient. Information content of the measurements were improved by adding polarization sensitivity. This involves transmitting a linearly polarized beam and separating the received backscatter into polarization components parallel and perpendicular to that beam (Churnside 2015). Even with this capability, the separation of backscatter and attenuation remains problematic and requires various assumptions and approximations.

Scientific application of elastic backscatter lidar began to flourish only in the last decade, largely reflecting the extensive deployments of the National Oceanic and Atmospheric Administration (NOAA) Fish Lidar (Churnside et al. 2001). This lidar was originally designed by James Churnside and colleagues for the detection and quantification of fish schools (Churnside et al. 1991; 2001; 2003), but they later turned their attention to application of the technique to retrieving ocean inherent optical properties. James Churnside's excellent review article (Churnside 2013) provides a detailed technical description of the elastic backscatter technique and an overview of the contributions made by his group and others on the modeling and interpretation of backscatter signals. Early scientific contributions with the NOAA lidar included several studies of subsurface plankton layers (e.g., Churnside & Ostrovsky 2005; Churnside & Donaghay 2009). More recently, the focus has been on overcoming the ambiguity in the elastic backscatter retrieval through bio-optical modeling. Churnside et al. (2014) employed a parameterization based on chlorophyll concentration to estimate the ratio of attenuation to backscatter, thereby reducing the

retrieval to solving for a single unknown, as is done for atmospheric aerosol retrievals (Fernald 1984). Churnside (2015) extended this bio-optical approach with an iterative scheme that enabled the retrieval of chlorophyll concentration in addition to particulate backscatter and diffuse attenuation. Churnside & Marchbanks (2015) applied the bio-optical retrieval to measurements of subsurface plankton layers in the Arctic, and Churnside (2016) employed it and radiometric measurements to estimate the vertical distribution of primary productivity.

The application of bio-optical modeling has transformed the elastic backscatter lidar technique from that of layer detection to a means of quantifying ocean properties. However, the impact of errors in the chlorophyll parameterization has yet to be assessed. The two parameterized unknowns, particulate backscatter and diffuse attenuation, can vary independently (e.g., with CDOM concentration) (Siegel et al. 2005). This affects attenuation but not backscatter and violates the retrieval assumptions. Unfortunately, retrieval errors accumulate as the retrieval proceeds downward through the profile, since the error at a particular depth interval is a function of the retrieval error at that depth interval and the accumulated error from intervals higher in the column. Also, the fundamental problem of absolute calibration of the signal still remains. Without calibration, the retrievals of particulate scattering are not possible. For the typical 300 m flight altitude of the NOAA lidar, the measured signals can be calibrated using preflight measurements and occasional ocean targets where scattering properties are uniform with depth. However, for the spaceborne application, the calibration of the ocean signal will vary significantly and rapidly with the optical depth of the overlying atmosphere (i.e., attenuation of the signal due to aerosol layers and tenuous clouds).

A significant leap in retrieval accuracy and information content has recently been made by applying the high spectral resolution lidar (HSRL) technique to ocean profiling. This technique

has been used for decades in ground-based (e.g., Shipley et al. 1997) and airborne (Esselborn et al. 2008; Hair et al. 2008) aerosol and cloud measurements. It is based on the difference in the wavelength distributions of backscatter from particles and molecules (**Figure 2**). By adding a spectral filter (e.g., interferometer) in the receiver optical path and directing particulate and molecular water scattering differentially to separate detectors, two signals are acquired that enable separating backscatter from pure seawater and suspended particles (e.g., phytoplankton). This separation of water and particulate backscatter is fundamental to the technique as it provides two lidar profiles from which to retrieve the two unknowns (i.e., particulate backscatter and diffuse attenuation), thus creating a well-posed rather than ill-posed retrieval (**Box 1**). Another equally important aspect of the HSRL technique concerns calibration. The technique inherently maintains calibration through the atmosphere and into the ocean. Accurate calibration and independent measurement of water and particulate backscatter ensures reliably accurate retrievals of the diffuse attenuation coefficient and particulate backscatter. Accurate calibration and optically separating the light scattered by water molecules and particles enables reliable retrievals of the both the diffuse attenuation coefficient and particulate backscatter.

The first extensive HSRL retrievals of diffuse attenuation, K_d, and particulate backscatter, b_{bp}, were made during the 2014 Ship-Aircraft Bio-Optical Research (SABOR) experiment (Hair et al. 2016, Schulien et al. 2017) and the 2015 and 2016 North Atlantic Aerosols and Marine Ecosystems Study (NAAMES) deployments. **Figure 3** shows atmospheric and ocean retrieval 'curtains' from a flight of the NASA HSRL-1 instrument during NAAMES. These data, acquired from a flight altitude of 9 km, illustrate the calibration advantage of the HSRL technique. Similar to a satellite viewing geometry, the optical path traveled by the photons to and from the ocean include attenuating layers of smoke in the free troposphere and marine aerosol in the boundary layer,

producing large variations in the strength of the ocean backscatter signals along the flight track. This would create a significant calibration challenge for the elastic backscatter technique, but not the HSRL (Hair et al. 2008; 2016).

The SABOR campaign provided an opportunity to compare HSRL-1 ocean retrieval products to independent measurements of the same properties. For example, **Figure 4a** shows an along-track comparison of the HSRL-derived K_d at 10 m depth and MODIS K_d values collected on the same day, with excellent agreement between products. The HSRL-1 ocean products also showed excellent agreement with optical properties measured at sea during SABOR. For example, **Figure 4 c and d** shows comparisons of depth-resolved b_{bp} values from HSRL-1 with near-coincident in situ data from optical profiling casts at the SABOR ship stations (Schulien et al. 2017). These comparisons with MODIS and in situ data have correlation coefficients ≥ 0.94 and slopes of ~1.0, giving high confidence in the HSRL technique.

Schulien et al. (2017) used in situ and HSRL-1 data from SABOR to quantify the value of vertically resolved measurements of b_{bp} and K_d for improving estimates of net primary production (NPP) relative to estimates based solely on the surface properties retrievable from passive ocean color data. Data from 17 SABOR sampling stations with lidar overflights indicated 'ocean color type' surface properties yielded estimates of water column integrated NPP that consistently underestimated values calculated with vertically-resolved data, with errors up to 54%. It should be further noted that vertical plankton structure during SABOR was modest at best and previous estimates of NPP errors associated with a wider range in vertical structure indicate that such errors can exceed 100% (Hill & Zimmerman 2010; Churnside 2015). Clearly, information on plankton vertical structure can significantly improve understanding of ocean plankton stocks, productivity, and carbon cycling.

As a final note for this section, we have largely focused the above discussion on lidar applications for retrieving surface and vertically-resolved ocean optical and plankton properties. Information on plankton vertical structure might further provide insight on physical mixing processes (Zawada et al. 2005). Specifically, the expectation is that particle concentrations in the active turbulent mixing layer will be homogeneous with depth. Accordingly, detection of subsurface scattering layers can be used to delineate the maximum depth of active mixing. This constraint on active mixing can be used as a global data set for testing physical mixing models and has the potential to significantly improve understanding on dynamic relationships between physics, plankton biomass, and bloom trajectories. However, there has also been a long interest in applying lidar technology to directly measure vertical profiles of ocean temperature and salinity (see, for instance, Hirschberg et al. 1984; Hickman et al. 1991; Fry et al. 1997; Popescu et al. 2004; Rudolf & Walther 2014; Liu et al. 2015). While much has been accomplished in terms of theoretical studies, development of instrument concepts, laboratory demonstrations, and sensitivity analyses, to our knowledge a practical lidar for measuring temperature or salinity has yet to be developed and deployed in the field from ship or aircraft. We therefore deemed these techniques as not yet mature enough for inclusion in our near-term vision for a spaceborne ocean lidar (**Sections 6 & 7**).

5. DAWN OF SATELLITE LIDAR IN OCEANOGRAPHY

The Coastal Zone Color Scanner (CZCS) was certainly not the best satellite sensor ever built to globally sample surface ocean properties, but it was the first. The idea of deriving plankton properties from remotely-detectable optical signals significantly pre-dates the CZCS and the concept had been demonstrated from aircraft. But, eventually the time comes to 'bite the bullet' and launch a proof-of-concept instrument into space. The launch of CZCS was that proof-of-

concept for ocean color and a landmark event. The dawn of the satellite lidar era in oceanography shares some parallels with this CZCS story in that the lidar approach was initially demonstrated with airborne sensors (in fact to a far greater degree for lidar than CZCS) and the first satellite demonstration was based on an instrument with limited capabilities. Unlike the CZCS story, however, the satellite lidar instrument was designed with no intention of retrieving properties of the ocean. That lidar was CALIOP.

As discussed above, CALIOP is a simple elastic backscatter lidar with emissions at 532 and 1064 nm, but in-water attenuation of the latter band is too great to provide any useful information on subsurface ocean properties. Since it was designed for atmospheric science applications, the 22.5 m vertical resolution of CALIOP measurements is very coarse for ocean applications, and the backscatter from the ocean surface created an artifact in the co-polarized subsurface data. Also, CALIOP simply lacks the advanced capabilities of an HSRL system, so it does not provide direct information required for independently separating the attenuation and backscattering components from the retrieved subsurface signal. However, what CALIOP does provide is a space-based measurement of an ocean signal at 532 nm from its cross-polarization channel. In addition, this ocean signal is measured at a constant viewing angle, has minimal atmospheric correction errors, is independent of solar angle, and is retrieved both day and night and through significant cloud and aerosol layers. The CALIOP orbit also has a 16-day repeat cycle that provides a globally representative sampling of ocean ecosystems (**Figure 5a**). Thus, while CALIOP was not the optimal lidar system for observing the ocean, it has not only yielded the first space-based proof-of-concept but significant scientific results as well.

The first challenge in using CALIOP data for oceanographic research was isolating the subsurface signal in a calibrated and quantitative manner. This was accomplished by employing

the ratio of cross-polarized to co-polarized signal returns (the "depolarization ratio"), which is very well calibrated through the atmosphere and ocean column due to the fact that both channels respond similarly to absorption and scattering losses. The algorithm employed the sum of the depolarization ratio from the first few bins below the ocean surface, an estimate of the backscatter from the ocean surface itself, K_d values from MODIS, and assumptions based on empirical data to generate a surface-weighted column estimate of b_{bp} (see Behrenfeld et al. 2013, Supplemental Materials for details).

The second challenge in using CALIOP data was to validate the ocean products. An ideal opportunity for this arose from a NASA funded airborne field campaign based in the Azores that was coupled to ship-based optical measurements being conducted as part of a UK Atlantic Meridional Transect cruise (Behrenfeld et al. 2013). The validation component of the lidar study was focused on ship, aircraft, MODIS Aqua, and CALIOP measurements b_{bp}. For the overall ship transect data, the study found a significantly better agreement between in situ b_{bp} and CALIOP retrievals ($r^2 = 0.54$) than for the MODIS ocean color retrievals ($r^2 = 0.13$ and 0.27 for different inversion algorithms). For the three aircraft flights of the campaign, CALIOP retrievals were well aligned with airborne HSRL-1 based b_{bp} data ($r^2 = 0.58$). Overall, these results were viewed as highly encouraging, given that the ship, aircraft, and satellite data diverged significantly in spatial resolution and were not temporally coincident.

Given the success of the field validation analysis, Behrenfeld et al (2013) then provided the first published global map of surface b_{bp} from a space based lidar and associated estimates of phytoplankton carbon biomass (C_{phyto}) and total particulate organic carbon (*POC*). These data were compared to MODIS-based b_{bp} values from the Garver-Siegel-Maritorena (GSM) inversion algorithm (Garver & Siegel 1997; Maritorena et al. 2002; Siegel et al. 2002) and the Quasi-

Analytical Algorithm (QAA) (Lee et al. 2002) and associated C_{phyto} (**Figure 5b**) and *POC* values. The CALIOP-based products exhibited similar global distributions and seasonal cycles as the MODIS based products, but also highlighted some inconsistencies. For example, the CALIOP global *POC* data showed a dual-mode frequency distribution similar to QAA, but with peaks at lower *POC* concentrations, and a low-*POC* peak (~45mg C m^3) that was consistent (but of smaller magnitude) with the peak in GSM data (see Figure S4 in Behrenfeld et al. 2013). One intent of these comparisons was to highlight how independent, active-sensor based retrievals of fundamental ocean properties may provide critical constraints for improving passive ocean color algorithms. An additional study attempted to retrieve vertically-resolved information in the ocean, but quantification of the profile data in terms of ecosystem parameter was not possible (Churnside et al. 2013).

The Behrenfeld et al. (2013) study focused on the utility of satellite lidar measurements for global ocean studies, but lidar measurements may be even more important for specific regions and science questions. One such example is an improved understanding of high latitude ecosystems. As noted above, high latitude regions present particularly challenging conditions for passive ocean color sensors. They tend to be plagued by persistent cloud cover, solar geometries change significantly during the year, and periods of polar night prevent any passive measurements at all over broad areas. Because of these challenges, incomplete ocean color records at high latitudes can completely miss critical events in plankton annual cycles. Here again, CALIOP has provided the first demonstration of how active lidar measurements from space can complement passive ocean color data to yield new scientific insights.

Over polar regions, convergence of the CALIOP orbit tracks provides its most dense spatial sampling (**Figure 5a**). Active sensing is particularly valuable here because the lidar measurements

can be made throughout the annual cycle, including polar night, and valid retrievals can be made between clouds and through clouds (for cloud optical depths <1). These advantages have allowed CALIOP to provide 1˚ binned spatial coverage comparable to that of MODIS in both the North and South Polar regions during late-spring to early-autumn months and better coverage from the late-autumn to early-spring period (**Figure 5d**). With these data, the recent Behrenfeld et al. (2016) study demonstrated that initiation of polar annual phytoplankton blooms generally occurs before conditions are suitable for passive ocean color retrievals. The CALIOP data further provided the clearest demonstration to date that annual cycles in polar phytoplankton biomass are driven, at the month time scale, by the rate of acceleration and deceleration in phytoplankton division rates. Accordingly, the climax of the bloom coincides with division rate maxima, rather than a decrease in division. The study also showed that interannual variability in the amplitude of the phytoplankton annual biomass cycle is related to the overall range in division rate between winter minima and summer maxima. Finally, the lidar data were used for a complete annual accounting of the relative contributions of ecological processes and ice cover changes to a decade of variations in polar phytoplankton biomass.

The lidar era in satellite oceanography has arrived.

6. A NEW LIGHT ON THE HORIZON

There are 1224 words in the previous section. Perhaps the three most important of these are 'proof-of-concept'. CALIOP does not represent a blueprint of what a satellite lidar can achieve for global ocean studies, but rather provides a tantalizing glimpse of where lidar measurements can take us. Transitioning a new measurement from ground-based observations to an on-orbit system has been the demise of many exciting new remote sensing concepts. The simple fact is that satellite missions are expensive, so launching a totally new technology is unnervingly risky

compared to iteratively improving an existing approach. CALIOP has unintentionally provided this key step from a field-verified 'good idea' to an on-orbit demonstrated capability. CALIOP is for satellite lidar what CZCS was for ocean color. It has shown us that an ocean signal is detectable from a space lidar. Now, it is time to think about what we can really achieve with a satellite lidar when it is actually built for ocean measurements.

There are 4 obvious targets for realizing major scientific advances from a space lidar, and each of these has airborne heritage: (1) improved vertical resolution of the detected signal, (2) expanded set of detection bands, and (3) additional laser emission wavelengths. Some of the science applications of these expanded capabilities are discussed in the following paragraphs.

Since the very beginning of the passive ocean color record, it has been recognized that the measurement was missing an essential property of the upper water column: the vertical distribution of suspended and dissolved constituents. CALIOP provided little information on vertical structure because of its coarse vertical sampling capability (22.5 m). An ocean-optimized space lidar can provide much finer vertical resolution than CALIOP (note that the ICESAT lidar measures ice surface topography at centimeter scales), but the trade-space needs to be carefully considered between spatial resolution and measurement precision. From airborne lidar sensors, water column vertical structure is clearly resolved at 1-3 meter resolution and a similar scale can be envisioned for a future satellite system. With such capabilities, phytoplankton and total suspended particulate distributions within the upper light field could be characterized globally to enable improved estimates of NPP and carbon stocks.

A counterpart to improved vertical resolution is increased penetration of the retrieved signal. The maximum depth from which valid retrievals can be achieved with a satellite lidar is a function of multiple factors, including laser pulse energy and repetition rate, laser emission

wavelength, telescope size, horizontal averaging, and the optical clarity of the water column. As a general 'rule of thumb', it is anticipated that an ocean-optimized satellite lidar will be able to retrieve valid ocean properties to approximately 2.5 to 3.0 optical depths[3]. Such retrieval depths have already been demonstrated with airborne lidar. Thus, a space lidar can detect plankton properties within as much as 65% of the euphotic zone. Importantly, phytoplankton within this upper layer are the dominant contributors to water column integrated primary production and vertical distribution within this layer is a significant source of uncertainty in ocean color based assessments of production (Platt & Sathyendranath 1988; Hill et al. 2012; Zhai et al. 2012). These studies clearly demonstrate the value of vertically-resolved lidar profiles for assessing ocean production and standing stocks, however, there are additional subsurface plankton features that are simply beyond the reach of lidar. Perhaps the most widely recognized of these is the deep chlorophyll maximum that is ubiquitous in the permanently stratified ocean (roughly the ocean region between 40^{o}N and 40^{o}S) and often lies very near the bottom of the photic zone (i.e., > 3.5 optical depths) (Cullen 1982; 2015). In many cases, the deep chlorophyll maximum predominantly reflects light-driven changes in phytoplankton chlorophyll:carbon (i.e., photoacclimation), rather than an increase in cell concentration (Fennel & Boss 2003). In such cases, this common feature can be effectively accounted for by assuming constant phytoplankton concentrations between 3.0 and 4.6 optical depths and applying a depth-dependent photoacclimation model to reconstruct the vertical structure in chlorophyll (e.g., Westberry et al. 2008). In other cases, however, the deep chlorophyll maximum can reflect significant changes in phytoplankton biomass. Routinely characterizing these features on a global scale will require

[3] Optical depth is defined by the product of physical depth and attenuation coefficient. Over one optical depth, for example, a radiant flux is reduced by 63%. For reference, the surface photic layer is commonly defined as 4.6 optical depths.

augmenting measurements from an advanced ocean lidar with additional technologies (see **Section 8**).

With respect to the detection bands, the most important next step in satellite lidar measurements will be to depart from the simple elastic scatter approach employed by CALIOP and include measurement bands that allow the direct separation of attenuation and backscattering coefficients. We have called attention to this issue multiple times in this review but believe it cannot be overstated. In previous analyses using CALIIOP data the separation of b_{bp} and K_d has been executed by using coincident ocean color data (Behrenfeld et al. 2013) or a simple empirical relationship (Behrenfeld et al. 2016). Clearly these approaches are less than satisfactory and a lidar-specific approach is needed. As discussed above (**Section 4**), the HSRL technique addresses this issue with additional detectors for distinguishing particulate and molecular backscattering. The significance of this advancement for ocean studies is that it will allow the lidar-retrieved geophysical properties to be independent of other satellite, field, or modeled data. One important application of such data is that the global sampling provided by a space lidar can provide an unprecedented test data set (in terms of temporal and spatial coverage) for improving ocean color geophysical retrievals. Currently, development and validation of ocean color algorithms rely on field collected data, which are sparse in time and terribly undersampled in space (**Figure 5c**). The benefit of the lidar data to ocean color retrievals is reciprocated by the improved spatial coverage of ocean color products that can allow extrapolation of lidar-based properties between orbit tracks.

Another exciting avenue for advancement is expansion of the detection waveband set to include measurements of lidar stimulated fluorescence. As discussed in Section 4, chlorophyll fluorescence measurements have been demonstrated with airborne lidar systems. A similar space-based fluorescence measurement could serve multiple scientific applications. First, the total

fluoresced light can be quantitatively related to pigment concentration. As incident sunlight causes significant changes in the quantum yield of fluorescence (a process referred to as non-photochemical quenching), lidar based assessments of pigment concentration will be most accurate for measurements made on the dark side of the Earth. These chlorophyll assessments, in turn, can be used to separate measured K_d values into that associated with phytoplankton pigments and that associated with other absorbing compounds. An important benefit of the lidar fluorescence measurements compared to passive fluorescence measurements is that, obviously, the passive measurements cannot be collected at night and thus suffer from uncertainties in non-photochemical quenching. In addition, the night-time lidar signal is based on fluorescence excitation of a known and fixed energy.

The benefit of a lidar chlorophyll fluorescence channel goes beyond simply an estimate of pigment concentration. Because the measurements are conducted both day and night with a fixed excitation energy, they permit an accurate quantification of the non-photochemical quenching (NPQ) response. Such data could enable more accurate descriptions of NPQ variability and thus be used to improve interpretations of ocean color base fluorescence data (again, the ocean color product then reciprocates by enabling spatial extension of lidar data). Lidar-based NPQ assessments could further be evaluated in terms of different types of phytoplankton assemblages, thus providing new insight on photoacclimation strategies. A final benefit from a lidar fluorescence channel is that it may provide information on iron-limited growth conditions. For this application, coincident ocean color data will be necessary. Iron stress in the presence of high macronutrients results in the synthesis of non-functional pigment-protein complexes that impact fluorescence quantum yields (Behrenfeld et al. 2006; Schrader et al. 2011; Behrenfeld & Milligan 2013). Quantum yields could be assessed by normalizing lidar measured fluorescence signals to

ocean color based pigment absorption at 532 nm (a product from a spectral inversion algorithm), potentially allowing detection of these unique complexes and thus mapping of iron stressed populations.

A final avenue for advancing ocean satellite lidar capabilities is increasing the number of laser spectral emissions to a 3-wavelength system of 355, 532, and 1064 nm. Multiple benefits can be envisioned from the addition of a 355 nm source. First, under oceanographic conditions of low CDOM, 355 nm can penetrate deeper into the water column than 532. Perhaps more importantly, the combination of 355 and 532 nm can provide critical information on water column constituents. On the absorption side of the house, CDOM exhibits an exponential increase in absorption with decreasing wavelength, while phytoplankton pigment absorption peaks in the visible wavelengths and tends to decrease in the near-ultraviolet. Thus, the 355 nm lidar measurement would enable some separation skill between absorption by CDOM and pigments. Differences in backscatter coefficients at 355 and 532 nm could similarly provide information on the slope of the particle size distribution, enabling improved assessments of phytoplankton biomass and total particulate carbon stocks. Here again it is important to emphasize the value of the HSRL technique, as the accuracy of these important advanced geophysical retrievals will be significantly compromised for a simple elastic scattering lidar.

In closing this section, we note that cloud and aerosol measurements from the ocean-optimized lidar described above would have powerful crosscutting applications in science at the ocean-atmosphere interface and atmospheric science in general. As highlighted in the Intergovernmental Report on Climate Change (Stocker 2014), clouds and aerosols are the largest drivers of uncertainty in estimates of the Earth's energy budget. Accurate measurements of aerosol extinction at 532 nm from a spaceborne HSRL would provide significantly improved estimates of

aerosol direct radiative effect compared to CALIOP (Thorsen & Fu 2015; Thorsen et al. 2017). The 532 nm extinction measurements would also provide a much improved satellite-based proxy for the concentration of cloud condensation nuclei (CCN) than is possible from passive sensors (Stier 2016), enabling advanced studies of aerosol-cloud interactions. A polarization-sensitive lidar with elastic backscatter channels at 1064 nm and HSRL channels at 532 nm would provide vertically-resolved curtains of aerosol type (i.e., identification of aerosol layers as marine aerosol, continental pollution, biomass smoke, or dust (Burton et al. 2012; 2014)) and lead to significant improvements to chemical transport models. The addition of HSRL channels at 355 nm would enable retrieval of aerosol effective radius and concentration (Müller et al. 2014), providing an even better proxy for CCN and valuable data for air quality applications. Finally, building on the work of Hu (2007) and Hu et al. (2007) using CALIOP data, coupling HSRL capability, polarization sensitivity, and finer vertical resolution in atmospheric measurements will significantly improve retrievals of cloud microphysical properties.

Table 1 is sort of a 'shopping list' summary of measurements enabled by the enhanced measurement capabilities described in this section. The first row in the table represents a CALIOP-like 'base-case', which is then followed by additional rows associated with an added capability and the value added for ocean and atmospheric science.

7. AN OPTIMIZED OCEAN-ATMOSPHERE SATELLITE LIDAR

We will now consider the design of an ocean-atmosphere optimized lidar with the measurement capabilities discussed in **Section 6**. To facilitate this description, we have provided a basic conceptual illustration of the design in **Figure 6**. To begin, the laser transmitter is 'seeded' by a low-power continuous-wave 1064 nm laser to ensure narrowband frequency-stable output as required for the HSRL technique. The fundamental 1064 nm output of the Pulsed Laser is

frequency doubled to 532 nm and tripled to 355 nm, providing output pulses at all three wavelengths. The receiver begins with a 1-1.5 m diameter telescope, similar to CALIOP and the European Space Agency (ESA) Aeolus wind lidar due to launch in late 2018. Light collected by the telescope is focused onto a field stop that defines the receiver field-of-view (FOV), which would closely match the divergence of the transmitted beam to minimize the collection of diffusely scattered sunlight while still collecting most of the backscattered laser light. Next, the light is re-collimated into a small-diameter beam (e.g., 2-3 cm) in the receiver and then dichroic beamsplitters are used to separate the various wavelengths for additional optical processing. Narrow-band solar rejection filters are employed in the various optical paths to reduce the magnitude of scattered sunlight remaining within the FOV. Polarizing beam cubes are further used to resolve the backscatter into polarization components that are parallel and perpendicular to the linear polarization of the transmitted laser pulses.

While there are alternate means of doing so, the HSRL technique is implemented here with interferometric optical filters that separate the received backscatter onto two detectors: one for which the measured backscatter is predominantly from water or air molecules ("Molecular Channel"), and the other which measures a combination of particulate and molecular backscatter ("Particulate Channel"). As discussed in **Section** 4, the two HSRL channels essentially provide two equations to solve for two unknowns: K_d and, in this case, the co-polarized component of b_{bp}. The cross-polarized component of b_{bp} is derived in a similar manner by also employing the signal measured on the cross-polarized detector. Because >99% of the backscatter from water molecules maintains the polarization of the transmitted laser pulse, it is convenient to implement the interferometer downstream of the polarization beamsplitter. Finally, the design includes a channel for measuring the chlorophyll fluorescence signal in the 680 nm region. Unlike past airborne

fluorescence lidars discussed in **Section 4**, the chlorophyll fluorescence signal will be normalized to the molecular backscatter measured via the HSRL technique and hence not rely on a separate water-Raman channel.

A critical feature in the design is spatial resolution. The vertical resolution would be ~2-3 m in the ocean, which reflects the laser temporal pulsewidth and the detection electronics bandwidth. The fundamental along-track horizontal resolution is determined by the receiver FOV and the laser repetition rate. For our concept, the FOV will be set to achieve a 90-m "footprint" diameter at the Earth's surface consistent with CALIOP. By setting the laser repetition rate to 150 Hz, the horizontal spacing between samples will be ~50 m, ensuring contiguous along-track horizontal sampling.

With only a 90-m swath, orbital geometry must be considered to appreciate horizontal sampling. Our envisioned lidar mission would have a sun-synchronous orbit similar to that of CALIOP, achieving a global sampling pattern like that in **Figure 5a.** CALIOP orbits the Earth ~15 times per day with spacing between consecutive orbits of 2752 km at the equator. The orbit pattern repeats every 16 days resulting in a sampling grid that is spaced by171 km at the equator and 111 at ±50˚ latitude. While this sampling is sparse by ocean color standards, the capability for sampling day or night, through aerosol layers and tenuous clouds, and in small holes between broken clouds means that monthly coverage of lidar data can actually rival that of ocean color **(Figure 5d)** and, in some seasons and latitudes, exceeds that of ocean color (Behrenfeld et al. 2016).

Clearly, the satellite lidar capabilities described above would provide unprecedented contributions to ocean and atmospheric science. The obvious next question is, does the technology exists to build an instrument with these capabilities? The answer to this question is a resounding 'yes'. Much effort has been expended in Europe and the US to develop HSRL capability for space.

The European Space Agency (ESA) has built a 355 nm HSRL scheduled to launch on the EarthCARE satellite in 2018. NASA has also focused significant resources on maturation of lidar technology, achieving all of the capabilities mentioned above and in **Section 6**. In fact, one lidar design for the ACE mission concept incorporates all of the capabilities discussed above except for the chlorophyll fluorescence channel. Other NASA programs have contributed to the maturation of that design, and an airborne prototype with the capabilities recommended herein is due for flight demonstration in 2018. The 'bottom line' is that there is no technical obstacle to the deployment of an ocean-atmosphere optimized satellite lidar by the mid 2020s.

8. VISION OF A VIRTUAL CONSTELLATION

Oceanographic research with satellite lidars is in its infancy. We hope this review has provided a useful description of the lidar technique, an interesting narrative of its history in marine applications, an exciting account of recent achievements with the satellite CALIOP sensor, and some forward-looking ideas on future scientific pursuits with an advanced satellite lidar based on current technological capabilities.

Throughout this review, we have contrasted lidar measurements with traditional ocean color observations, but the most important message to take from these comparisons is that each approach has its strengths and weaknesses. In constructing a vision for future global ocean observing, we have learned from the A-train experience to capitalize on synergies between measurement approaches. An ocean optimized HSRL-type satellite lidar will alone revolutionize our understanding of ocean ecosystems, but the benefits of such a mission are greatly expanded if coupled to advanced ocean color observations (such as envisioned for the PACE mission sensor). Synergies from this pairing maximize global spatial and temporal data coverage, introduce the vertical dimension into ecosystem characterizations, and allow cross-instrument data comparisons

for algorithm development, improved ocean color atmospheric corrections, and an expansion in the diversity of retrieved geophysical properties.

Adding a scanning polarimeter to this emerging constellation yields additional synergies. A polarimeter would provide valuable information for spatially extending the detailed atmospheric characterization from the lidar 'curtains', and together these data will further improve ocean color atmospheric corrections. Polarimetry can also provide additional information on particle characteristics within the upper water column (Loisel et al. 2008). Reciprocating, the ocean color measurements provide constraints on water leaving contributions to the signal measured by the polarimeter.

One additional piece that can be added to our measurement constellation is a global array of in situ bio-geo-Argo floats. In addition to providing sustained and coincident field validation data for the satellite sensors, these autonomous assets can address a fundamental constraint on all known remote sensing technologies: there is a depth-limit to ocean signals observable from space. Satellite lidar can push this detection limit to ~3 optical depths, but significant ecosystem and biogeochemical processes occur below this depth. A bio-geo-Argo array could provide a global sampling of these deeper properties and, while not at the spatial resolution of remote sensing data, a means for extending satellite observables to the deep sea.

Figure 7 is an artistic rendering of this virtual ocean observing constellation. If the PACE mission is launched in its desired two-instrument configuration, we would be halfway to realizing this broader vision. Discussions are also underway regarding developing a global bio-geo-Argo array and significant investments are already being made in deployments (e.g., the Southern Ocean Carbon and Climate Observations and Modeling (SOCCOM) program (https://soccom.princeton.edu). The final piece is an advanced ocean lidar.

DISCLOSURE STATEMENT

To be completed later

ACKNOWLEDGMENTS

To be completed later.

LITERATURE CITED

Alvain S, Moulin C, Dandonneau Y, Breon F. 2005. Remote sensing of phytoplankton groups in case 1 waters for global SeaWiFS imagery. *Deep-Sea Res. I* 52:1989–2004

Antoine D, André J-M, Morel A. 1996. Oceanic primary production 2. Estimation at global scale from satellite (coastal zone color scanner) chlorophyll. *Global Biogeochem. Cycles* 10:57-69

Behrenfeld MJ, Falkowski PG. 1997. Photosynthetic rates derived from satellite-based chlorophyll concentration. *Limnol. Oceanogr.* 42:1-20

Behrenfeld MJ, Randerson JT, McClain CR, Feldman GC, Los SO, Tucker CJ, Falkowski PG, Field CB, Frouin R, Esaias WE, Kolber DD, Pollack NH. 2001. Biospheric primary production during an ENSO transition. *Science* 291:2594-7

Behrenfeld MJ, Boss E, Siegel DA, Shea DM. 2005. Carbon-based ocean productivity and phytoplankton physiology from space. *Global Biogeochem. Cycles* 19(1)

Behrenfeld MJ, Worthington K, Sherrell RM, Chavez FP, Strutton P, McPhaden M, Shea DM. 2006. Controls on tropical Pacific Ocean productivity revealed through nutrient stress diagnostics. *Nature* 442:1025-8

Behrenfeld MJ, Westberry TK, Boss E, O'Malley RT, Siegel DA, Wiggert JD, Franz BA, McClain CR, Feldman GC, Doney SC, Moore JK, Dall'Olmo G, Milligan AJ, Lima I, Mahowald N. 2009. Satellite-detected fluorescence reveals global physiology of ocean phytoplankton. *Biogeosciences* 6:779-94

Behrenfeld MJ, Hu Y, Hostetler CA, Dall'Olmo G, Rodier SD, Hair JW, Trepte CR. 2013. Space-based lidar measurements of global ocean carbon stocks. *Geophys. Res. Lett.* 40(16):4355-60

Behrenfeld MJ, Milligan AJ. 2013. Photophysiological expressions of iron stress in phytoplankton. *Ann. Rev. Mar. Sci.* 5:217-46

Behrenfeld MJ, Hu Y, O'Malley RT, Boss ES, Hostetler CA, Siegel DA, Sarmiento JL, Schulien J, Hair JW, Lu X, Rodier S, Scarino AJ. 2016. Annual boom-bust cycles of polar phytoplankton biomass revealed by space-based lidar. *Nat. Geosci* 10:118-22

Billard B, Abbot RH, Penny MF. 1986. Airborne estimation of sea turbidity parameters from the WRELADS laser airborne depth sounder. *Appl. Opt.* 25(13):2080-8

Boss E, Pegau WS. 2001. Relationship of light scattering at an angle in the backward direction to the backscattering coefficient. *Appl. Opt.* 40(30):5503-07

Bracher A, Vountas M, Dinter T, Burrows JP, Röettgers R, Peeken I. 2009. Quantitative observation of cyanobacteria and diatoms from space using PhytoDOAS on SCIAMACHY data. *Biogeosciences* 6(5):751–64

Bristow M, Nielsen D, Bundy D, Furtek R. 1981. Use of water Raman emission to correct airborne laser fluorosensor data for effects of water optical attenuation. *Appl. Opt.* 20(17):2889-2906

Bunkin AF, Surovegin AL. 1992. Lidar-aided measurement of phytoplankton chlorophyll and underwater scattering layers. *System* 50:1

Burton SP, Ferrare RA, Hostetler CA, Hair JW, Rogers RR, Obland MD, Butler CF, Cook AL, Harper DB, Froyd KD. 2012. Aerosol classification using airborne High Spectral Resolution Lidar measurements-methodology and examples. *Atmos. Meas. Tech.* 5(1):73

Burton SP, Vaughan MA, Ferrare RA, Hostetler CA. 2014. Separating mixtures of aerosol types in airborne High Spectral Resolution Lidar data. *Atmos. Meas. Tech. 7*(2):419

Chekalyuk AM, Hoge FE, Wright CW, Swift RN, Yungel JK. 2000. Airborne test of laser pump-and-probe technique for assessment of phytoplankton photochemical characteristics. *Photosynth. Res.* 66(1-2):45-56.

Churnside JH, Wilson JJ, Tatarskii VV. 1997. Lidar profiles of fish schools. *Appl. Opt.* 36(24):6011-20

Churnside JH, Wilson JJ, Tatarskii VV. 2001. Airborne lidar for fisheries applications. *Opt. Eng.* 40(3):406-4

Churnside JH, Demer DA, Mahmoudi B. 2003. A comparison of lidar and echosounder measurements of fish schools in the Gulf of Mexico. *ICES J. Mar. Sci.* 60(1):147-54

Churnside JH, Ostrovsky LA. 2005. Lidar observation of a strongly nonlinear internal wave train in the Gulf of Alaska. *Int J Remote Sens.* 26(1):167-7

Churnside JH, Donaghay PL. 2009. Thin scattering layers observed by airborne lidar. *ICES J. Mar. Sci.*

Churnside JH, McCarty BJ, Lu X. 2013. Subsurface ocean signals from an orbiting polarization lidar. *Rem. Sens.* 5(7):3457-75

Churnside JH, Sullivan JM, Twardowski MS. 2014. Lidar extinction-to-backscatter ratio of the ocean. *Opt. Express* 22(15):18698-706

Churnside JH. 2015. Bio-optical model to describe remote sensing signals from a stratified ocean. *J. Appl. Remote Sens.* 9(1):095989

Churnside JH, Marchbanks RD. 2015. Subsurface plankton layers in the Arctic Ocean. *Geophys. Res. Lett.* 42(12):4896-4902

Churnside JH. 2016. Airborne lidar estimates of photosynthesis profiles. In *Geoscience and Remote Sensing Symposium (IGARSS), 2016 IEEE International* (pp. 3777-3780). IEEE

Cullen JJ. 1982. The deep chlorophyll maximum: comparing vertical profiles of chlorophyll a. *Can. J. Fish. Aq. Sci.* 39:791–803

Cullen JJ. 2015. Subsurface chlorophyll maximum layers: Enduring enigma or mystery solved? *Annu. Rev. Mar. Sci.* 7(1):207-39

DeVries T, Primeau F, Deutsch C. 2012. The sequestration efficiency of the biological pump. *Geophys. Res. Lett.* 39(13)

Esselborn M, Wirth M, Fix A, Tesche M, Ehret G. 2008. Airborne high spectral resolution lidar for measuring aerosol extinction and backscatter coefficients. *Appl. Opt.* 47(3):346-58

Falkowski PG, Kim Y, Kolber Z, Wilson C, Wirick C, Cess R. 1992. Natural Versus Anthropogenic Factors Affecting Low-Level Cloud Albedo over the North Atlantic. *Science* 256(5061):1311-3

Falkowski PG, Barber RT, Smetacek V. 1998. Biogeochemical controls and feedbacks on ocean primary production. *Science* 281(5374):200–6

Fennel K, Boss E. 2003. Subsurface maxima of phytoplankton and chlorophyll: Steady state solutions from a simple model. *Limnol. Oceanogr.* 48(4):1521-34

Fernald FG. 1984. Analysis of atmospheric lidar observations- Some comments. *Appl. Opt.* 23(5):652-3

Field CB, Behrenfeld MJ, Randerson JT, Falkowski PG. 1998. Primary production of the biosphere: Integrating terrestrial and oceanic components. *Science* 281:237-40

Fry ES, Emery Y, Quan X, Katz JW. 1997. Accuracy limitations on Brillouin lidar measurements of temperature and sound speed in the ocean. *Appl. Opt.* 36(27):6887-94

Gantt B, Meskhidze N. 2013. The physical and chemical characteristics of marine primary organic aerosol: a review. *Atmos. Chem. Phys.* 13(8):3979-96

Garver SA, Siegel DA. 1997. Inherent optical property inversion of ocean color spectra and its biogeochemical interpretation: I. Time series from the Sargasso Sea. *J. Geophys. Res.* 102(C8):18607-25

Hair JW, Hostetler CA, Cook AL, Harper DB, Ferrare RA, Mack TL, Welch W, Izquierdo LR, Hovis FE. 2008. Airborne high spectral resolution lidar for profiling aerosol optical properties. *Appl. Opt.* 47(36):6734-52

Hair J, Hostetler C, Hu Y, Behrenfeld M, Butler C, Harper D, Hare R, Berkoff T, Cook A, Collins J, Stockley N. 2016. Combined Atmospheric and Ocean Profiling from an Airborne High Spectral Resolution Lidar. *EPJ Web of Conferences* 119:22001. EDP Sciences

Hickman GD, Harding JM, Carnes M, Pressman A, Kattawar GW, Fry ES. 1991. Aircraft laser sensing of sound velocity in water: Brillouin scattering. *Remote Sens. Environ.* 36(3):165-78

Hill VJ, Zimmerman RC. 2010. Estimates of primary production by remote sensing in the Arctic Ocean: Assessment of accuracy with passive and active sensors. *Deep-Sea Res. I* 57(10): 1243-54

Hill VJ, Matrai PA, Olson E, Suttles S, Steele M, Codispoti LA, Zimmerman RC. 2013. Synthesis of integrated primary production in the Arctic Ocean: II. In situ and remotely sensed estimates. *Prog. Oceanogr.* 110:107-25

Hirschberg JG, Byrne JD, Wouters AW, Boynton GC. 1984. Speed of sound and temperature in the ocean by Brillouin scattering. *Appl. Opt.* 23(15):2624-8

Hoge FE, Swift RN. 1981. Airborne simultaneous spectroscopic detection of laser-induced water Raman backscatter and fluorescence from chlorophyll a and other naturally occurring pigments. *Appl. Opt.* 20(18):3197-3205

Hoge FE, Wright CW, Krabill WB, Buntzen RR, Gilbert GD, Swift RN, Yungel JK, Berry RE. 1988. Airborne lidar detection of subsurface oceanic scattering layers. *Appl. Opt.* 27(19):3969-77

Hoge FE, Swift R, Yungel J. 1995. Oceanic radiance model development and validation: application of airborne active-passive ocean color spectral measurements. *Appl. Opt.* 34(18):3468-76

Hoge FE, Lyon PE, Swift RN, Yungel JK, Abbott MR, Letelier RM, Esaias WE. 2003. Validation of Terra-MODIS phytoplankton chlorophyll fluorescence line height. I. Initial airborne lidar results. *Appl. Opt.* 42(15):2767-71

Hoge FE, Lyon PE, Wright CW, Swift RN, Yungel JK. 2005. Chlorophyll biomass in the global oceans: airborne lidar retrieval using fluorescence of both chlorophyll and chromophoric dissolved organic matter. *Appl. Opt*. 44(14):2857-62

Hu Y. 2007. Depolarization ratio–effective lidar ratio relation: Theoretical basis for space lidar cloud phase discrimination. *Geophys. Res. Lett.* 34(11)

Hu Y, Vaughan M, McClain C, Behrenfeld M, Maring H, Anderson D, Sun-Mack S, Flittner D, Huang J, Wielicki B, Minnis P. 2007. Global statistics of liquid water content and effective number concentration of water clouds over ocean derived from combined CALIPSO and MODIS measurements. *Atmos. Chem. Phys. 7*(12):3353-9

Hu Y. 2009. Ocean, Land and Meteorology Studies Using Space-Based Lidar Measurements. 5th WSEAS International Conference on Remote Sensing (REMOTE'09), Genova, Italy. https://ntrs.nasa.gov/search.jsp?R=20090037431

Jacox MG, Edwards CA, Kahru M, Rudnick DL, Kudela RM. 2015. The potential for improving remote primary productivity estimates through subsurface chlorophyll and irradiance measurement. *Deep-Sea Res. II* 112:107-16

Kato S, Rose FG, Sun-Mack S, Miller WF, Chen Y, Rutan DA, Stephens GL, Loeb NG, Minnis P, Wielicki BA, Winker DM. 2011. Improvements of top-of-atmosphere and surface irradiance computations with CALIPSO-, CloudSat-, and MODIS-derived cloud and aerosol properties. *J. Geophys. Res: Atmospheres* 116(D19)

Kim HH. 1973. New algae mapping technique by the use of an airborne laser fluorosensor. *Appl. Opt.* 12(7):1454-9

Kostadinov TS, Siegel DA, Maritorena S. 2010. Global variability of phytoplankton functional types from space: assessment via the particle size distribution. *Biogeosciences* 7(10):3239–57

Lee Z, Carder KL, Arnone RA. 2002. Deriving inherent optical properties from water color: A multi-band quasi-analytical algorithm for optically deep waters. *Appl. Opt.* 41:5755-72

Lee, Z.P., Darecki, M., Carder, K.L., Davis, C.O., Stramski, D. and Rhea, W.J., 2005. Diffuse attenuation coefficient of downwelling irradiance: An evaluation of remote sensing methods. *Journal of Geophysical Research: Oceans*, *110*(C2)

Lin H, Kuzminov FI, Park J, Lee S, Falkowski PG, Gorbunov MY. 2016. The fate of photons absorbed by phytoplankton in the global ocean. *Science* 351(6270):264-7

Liu J, Shi J, He X, Chen X, Liu D. 2015. Comparison of three technique of Brillouin lidar for remote sensing of the ocean. *Opt. Commun.* 352:161-5

Loisel H, Duforet L, Dessailly D, Chami M, Dubuisson P. 2008. Investigation of the variations in the water leaving polarized reflectance from the POLDER satellite data over two biogeochemical contrasted oceanic areas. *Opt. Express* 16(17):12905-18

Maritorena S, Siegel DA, Peterson AR. 2002. Optimization of a semianalytical ocean color model for global-scale applications. *Appl. Opt*. 41:2705–14

Martin JH, Coale KH, Johnson KS, Fitzwater SE, Gordon RM, Tanner SJ, Hunter CN, Elrod VA, Nowicki JL, Coley TL, Barber RT, Lindley S, Watson AJ, Van Scoy K, Law CS, Liddicoat MI, Ling R, Stanton T, Stockel J, Collins C, Anderson A, Bidigare R, Ondrusek M, Latasa M, Millero FJ, Lee K, Yao W, Zhang JZ, Friederich G, Sakamoto C, Chavez F, Buck K, Kolber Z, Greene R, Falkowski P, Chisholm SW, Hoge F, Swift R, Yungel J, Turner S, Nightingale P, Hatton A, Liss P, Tindale NW. 1994. Testing the iron hypothesis in ecosystems of the equatorial Pacific Ocean. *Nature* (371):123-9

McClain CR. 2009. A decade of satellite ocean color observations. *Annu. Rev. Mar. Sci.* 1:19–42

Meskhidze N, Nenes A. 2006. Phytoplankton and Cloudiness in the Southern Ocean. *Science* 314:1419-23

Müller D, Hostetler CA, Ferrare RA, Burton SP, Chemyakin E, Kolgotin A, Hair JW, Cook AL, Harper DB, Rogers RR, Hare RW. 2014. Airborne Multiwavelength High Spectral Resolution Lidar (HSRL-2) observations during TCAP 2012: vertical profiles of optical and microphysical properties of a smoke/urban haze plume over the northeastern coast of the US. *Atmos. Meas. Tech.*

O'Malley RT, Behrenfeld MJ, Westberry TK, Milligan AJ, Shang S, Yan J. 2014. Geostationary satellite observations of dynamic phytoplankton photophysiology. *Geophys. Res. Lett.* 41(14):5052-9

Platt T, Sathyendranath S. 1988. Oceanic primary production: estimation by remote sensing at local and regional scales. *Science* 241(4873):1613-20

Poole LR, Esaias WE. 1982. Water Raman normalization of airborne laser fluorosensor measurements: a computer model study. *Appl. Opt.* 21(20):3756-61

Popescu A, Schorstein K, Walther T. 2004. A novel approach to a Brillouin–LIDAR for remote sensing of the ocean temperature. *Appl. Phys. B.* 79(8):955-61

Rudolf A, Walther T. 2014. Laboratory demonstration of a Brillouin lidar to remotely measure temperature profiles of the ocean. *Opt. Eng.* 53(5):051407

Ryu JH, Han HJ, Cho S, Park YJ, Ahn YH. 2012. Overview of geostationary ocean color imager (GOCI) and GOCI data processing system (GDPS). *Ocean Sci. J.* 47(3):223–33

Sadeghi A, Dinter T, Vountas M, Taylor B, Altenburg-Soppa M, Bracher A. 2012. Remote sensing of coccolithophore blooms in selected oceanic regions using the PhytoDOAS method applied to hyper-spectral satellite data. *Biogeosciences* 9(6):2127–43

Sathyendranath S, Platt T. 1989. Remote sensing of ocean chlorophyll: consequence of nonuniform pigment profile. *Appl. Opt.* 28(3):490-5

Sathyendranath S, Aiken J, Alvain S, Barlow R, Bouman H, Bracher A, Brewin R, Bricaud A, Brown CW, Ciotti AM, Clementson LA. 2014. Phytoplankton functional types from Space. In Reports of the International Ocean-Colour Coordinating Group (IOCCG) 15:1-156

Schrader PS, Milligan AJ, Behrenfeld MJ. 2011. Surplus photosynthetic antennae complexes underlie diagnostics of iron limitation in a cyanobacterium. *PloS One* 6(4):e18753

Schulien JA, Behrenfeld MJ, Hair JW, Hostetler CA, Twardowski MS. 2017. Vertically-resolved phytoplankton carbon and net primary production from a High Spectral Resolution Lidar. *Opt. Express,* Submitted

Shipley ST, Tracy DH, Eloranta EW, Trauger JT, Sroga JT, Roesler FL, Weinman JA. 1983. High spectral resolution lidar to measure optical scattering properties of atmospheric aerosols. 1: Theory and instrumentation. *Appl. Opt.* 22(23):3716-24

Siegel DA, Maritorena S, Nelson NB, Hansell DA, Lorenzi-Kayser M. 2002. Global distribution and dynamics of colored dissolved and detrital organic materials. *J. Geophys. Res*: *Oceans* 107(C12)

Siegel DA, Maritorena S, Nelson NB, Behrenfeld MJ. 2005. Independence and interdependencies of global ocean color properties: Reassessing the bio-optical assumption. *J. Geophys. Res*: *Oceans* 110(C7)

Silsbe GM, Behrenfeld MJ, Halsey KH, Milligan AJ, Westberry TK. 2016. The CAFE model: A net production model for global ocean phytoplankton. *Global Biogeochem. Cycles* 30:1756-77

Smart JH, Kwon KHK. 1996. Comparisons between in-situ and remote sensing estimates of diffuse attenuation profiles. In CIS Selected Papers: Laser Remote Sensing of Natural Waters--From Theory to Practice, pp. 100-109. International Society for Optics and Photonics.

Stier P. 2016. Limitations of passive remote sensing to constrain global cloud condensation nuclei. *Atmos. Chem. Phys.* 16(10):6595-6607

Stocker T. ed., 2014. *Climate change 2013: the physical science basis: Working Group I contribution to the Fifth assessment report of the Intergovernmental Panel on Climate Change*. Cambridge University Press

Stramska M, Stramski D. 2005. Effects of a nonuniform vertical profile of chlorophyll concentration on remote-sensing reflectance of the ocean. *Appl. Opt.* 44(9):1735-47

Thorsen TJ, Fu Q. 2015. CALIPSO-inferred aerosol direct radiative effects: Bias estimates using ground-based Raman lidars. *J. Geophys. Res: Atmospheres*

Thorsen TJ, Ferrare RA, Hostetler CA, Vaughan MA, Hair JW, Fu Q. 2017. Towards quantifying global aerosol direct radiative effects using lidar: detection sensitivity. *Geophys. Res. Lett.* in preparation

Vasilkov AP, Goldin YA, Gureev BA, Hoge FE, Swift RN, Wright CW. 2001. Airborne polarized lidar detection of scattering layers in the ocean. *Appl. Opt.* 40(24):4353-64

Werdell PJ, Franz BA, Bailey SW, Feldman GC, Boss E, Brando VE, Dowell M, Hirata T, Lavender SJ, Lee Z, Loisel H, Maritorena S, Mélin F, Moore TS, Smyth TJ, Antoine D, Devred E, d'Andon O, Mangin A. 2013. Generalized ocean color inversion model for retrieving marine inherent optical properties. *Appl. Opt.* 52(10):2019-37

Westberry TK, Behrenfeld MJ, Siegel DA, Boss E. 2008. Carbon-based primary productivity modeling with vertically resolved photoacclimation. *Global Biogeochem. Cycles*. 22(2)

Westberry TK, Behrenfeld MJ, Milligan AJ, Doney SC. 2013. Retrospective satellite ocean color analysis of purposeful and natural ocean iron fertilization. *Deep-Sea Res. I* 73:1-16

Winker DM, Vaughan MA, Omar A, Hu Y, Powell KA, Liu Z, Hunt WH, Young SA. 2009. Overview of the CALIPSO mission and CALIOP data processing algorithms. *J. Atmos. Oceanic Technol.* 26(11):2310-23

Yoder JA, Aiken J, Swift RN, Hoge FE, Stegmann PM. 1993. Spatial variability in near-surface chlorophyll a fluorescence measured by the Airborne Oceanographic Lidar (AOL). *Deep-Sea Res. Part II* 40(1-2):37-53

Zawada DG, Zaneveld J, Ronald V, Boss E, Gardner WD, Richardson MJ, Mishonov AV. 2005. A comparison of hydrographically and optically derived mixed layer depths. *J. Geophys. Res*: *Oceans* 110(C11)

Zhai L, Gudmundsson K, Miller P, Peng W, Guðfinnsson H, Debes H, Hátún H, White GN, Walls RH, Sathyendranath S, Platt T. 2012. Phytoplankton phenology and production around Iceland and Faroes. Cont. Shelf Res. 37:15-25

SIDEBAR - BOX 1

HSRL: TWO MEASUREMENTS, TWO UNKNOWNS

HSRL designs vary from instrument to instrument, but the fundamental approach is the same. We will consider here the simplest of HSRL architectures where there are two detection channels. One of these channels is more sensitive to particulate backscatter from the ocean (the middle peak in **Figure 2**) and one is more sensitive to molecular backscatter from seawater itself (the right and left peaks in **Figure 2**). This separation of the backscatter signal is accomplished in the lidar receiver (**Figure 1)** with a spectral filter (e.g., an interferometer) that has a well characterized frequency response. The two time-resolved signals are combined to form two profiles proportional to backscatter at 180˚. The first of these derived profiles, $S_M(z)$, represents photons backscattered by water (β_M):

$$S_M(z) = C_M \beta_M \exp\left[-2\int_0^z K_d(z')dz'\right](Atmos.Transmission)^2 \qquad (1)$$

where the integral of K_d and the square of the atmospheric transmission account for the attenuation that the transmitted and backscattered photons undergo along their optical paths. C_M is a channel-specific instrument constant that incorporates factors like laser energy, telescope area, and the efficiency of receiver components. The second profile, $S_P(z)$, represents photons backscattered by suspended particles in the ocean (β_P) and likewise attenuated by the ocean (K_d) and atmosphere:

$$S_P(z) = C_P \beta_P(z) \exp\left[-2\int_0^z K_d(z')dz'\right](Atmos.Transmission)^2 \qquad (2)$$

where C_P is the instrument constant for the second channel. Because the density of seawater molecules is relatively constant in the near-surface ocean, the value of β_M is well known. Thus, the value of K_d can be calculated from changes in $S_M(z)$ from one depth interval to the next through the water column:

$$K_d(z) = \left[-\frac{1}{2}\frac{d}{dz}\ln(S_M(z))\right] \quad (3)$$

Importantly, the influence of K_d and atmospheric transmission are the same for $S_P(z)$ and $S_M(z)$. Consequently, these two terms cancel in the ratio $S_P(z)$:$S_M(z)$, allowing the attenuation-corrected profile of particulate backscatter at 180˚ to be calculated as:

$$\beta_P(z) = \beta_M \left[\frac{C_M}{C_P}\right]\left[\frac{S_P(z)}{S_M(z)}\right] \quad (4)$$

where the only scaling factors required are estimates of β_M (well-known) and the C_M:C_P ratio (which is easily calibrated with high accuracy). β_P is then scaled to hemispheric backscatter, b_{bp}, following Boss & Pegau (2001).

In summary, the power of the HSRL technique is that it provides two measurements to solve for two unknowns and requires only relative (i.e., the C_M:C_P ratio), rather than absolute, calibration. This contrasts critically from the elastic backscatter lidar technique, which provides the combined $S_P(z)+S_M(z)$ profile only and therefore requires absolute calibration, correction for the atmospheric transmission, and either ancillary data or model assumptions on the relationship between b_{bp} and K_d to retrieve either one.

TABLES

Table 1. Summary of the increase in science value with capability from the CALIOP base case.

	Added Capability	Added Value to Ocean Science	Added Value to Atmospheric/Land Science
CALIOP Equivalent	CALIOP: • Elastic backscatter technique at 532 and 1064 nm • Depolarization at 532 nm • Vertical resolution: 23-m (30-m) ocean (atmosphere)	• Surface-weighted b_{bp} and K_d (not independent) • Sampling through aerosol layers and tenuous cloud • Sampling regardless of sun angle • Monthly coverage statistics ~50% of those for ocean color for 1˚x1˚ bins • Day-night comparisons possible	• Cloud vertical distribution and microphysical properties relevant to radiation budget studies • Aerosol vertical distribution and scattering properties relevant to radiation budget and air quality studies. Accuracy limited by retrieval assumptions and loss of calibration with penetration into atmosphere. • Crude aerosol typing with high uncertainty
Above Plus	Above plus: + <3-m vertical resolution	• Crude estimates of profile-average K_d; unknown error due to vertical variability in K_d and b_{bp}. • Crude b_{bp} profiling capability: calibration will be an issue	• Enhanced capability for cloud microphysical retrievals
Above Plus	Above plus: + HSRL at 532 nm + Depolarization at 1064 nm	• Accurate independent profiles of b_{bp} and K_d at 532 nm • Calibration maintained through ocean column. • Products scalable to C_{phyto}, POC, and chlorophyll concentration via empirical relationships • Vertically-resolved estimates of NPP	• Accurate profiles of aerosol extinction and backscatter through entire profile and into the BL. • Improved satellite CCN proxies • Improved air quality estimates • Significant skill in aerosol typing and partitioning optical depth by type. • More accurate estimates of optical thickness of tenuous clouds. • Advanced cloud microphysical retrievals
Above Plus	Above plus: + Chl Fluorescence	• NPQ • Iron stress	
Above Plus	Above plus: + HSRL at 355 nm + Depolarization at 355 nm	• Accurate independent profiles of b_{bp} and K_d at 532 and 355 nm • Independent estimates of CDOM and pigment absorption • Information on the slope of the plankton size distribution • Increased accuracy in vertically-resolved NPP	• Aerosol effective radius and concentration • Enhanced satellite CCN proxies • Enhanced air quality estimates • Enhanced skill in aerosol typing, e.g., discriminating between fresh and aged smoke

FIGURES

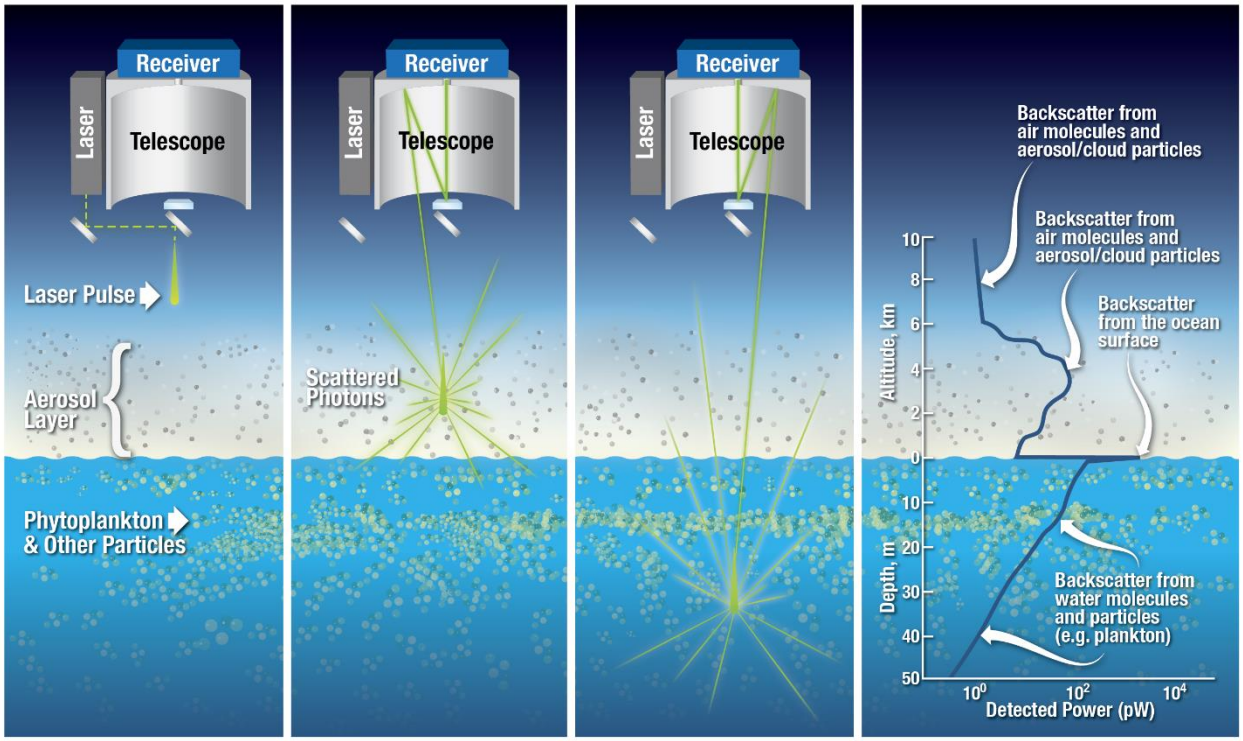

Figure 1. Illustration of the lidar time-of-flight ranging technique. (a)The laser transmits a short (e.g., 15 ns) pulse of laser light which is directed downward. (b) As the laser pulse travels toward Earth, photons are scattered from air molecules and cloud/aerosol particles in the atmosphere. (c) Shortly thereafter, the pulse penetrates the ocean where photons are also scattered by water molecules and suspended particles. Some of the scattered photons in the atmosphere and ocean are intercepted by the telescope, and the magnitude of this signal is recorded as a function of time by detectors located in the receiver. (d) Using the speed of light, time is converted to distance, creating a vertically-resolved profile of received backscatter.

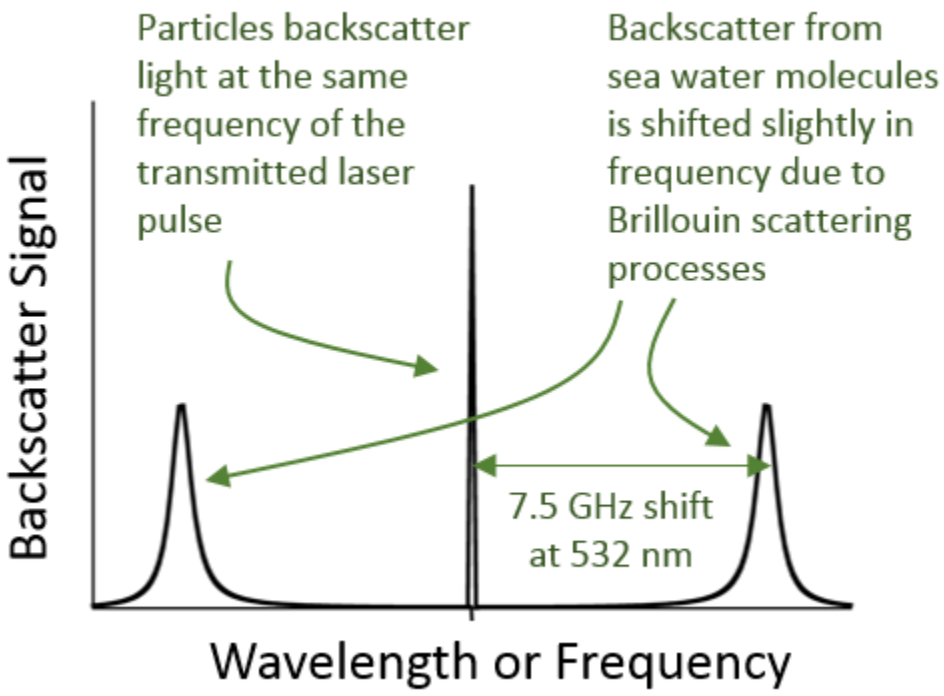

Figure 2. The HSRL technique **(Box 1)** relies on the spectral separation between 180˚ backscatter from seawater and suspended particles (e.g., phytoplankton). The spectrum of particulate backscatter is nearly identical to that of the transmitted single-frequency laser pulse. Molecular backscatter, on the other hand, is shifted (~7.5 GHz at 532 nm) and broadened by Brillouin scattering processes (Hickman et al. 1991).

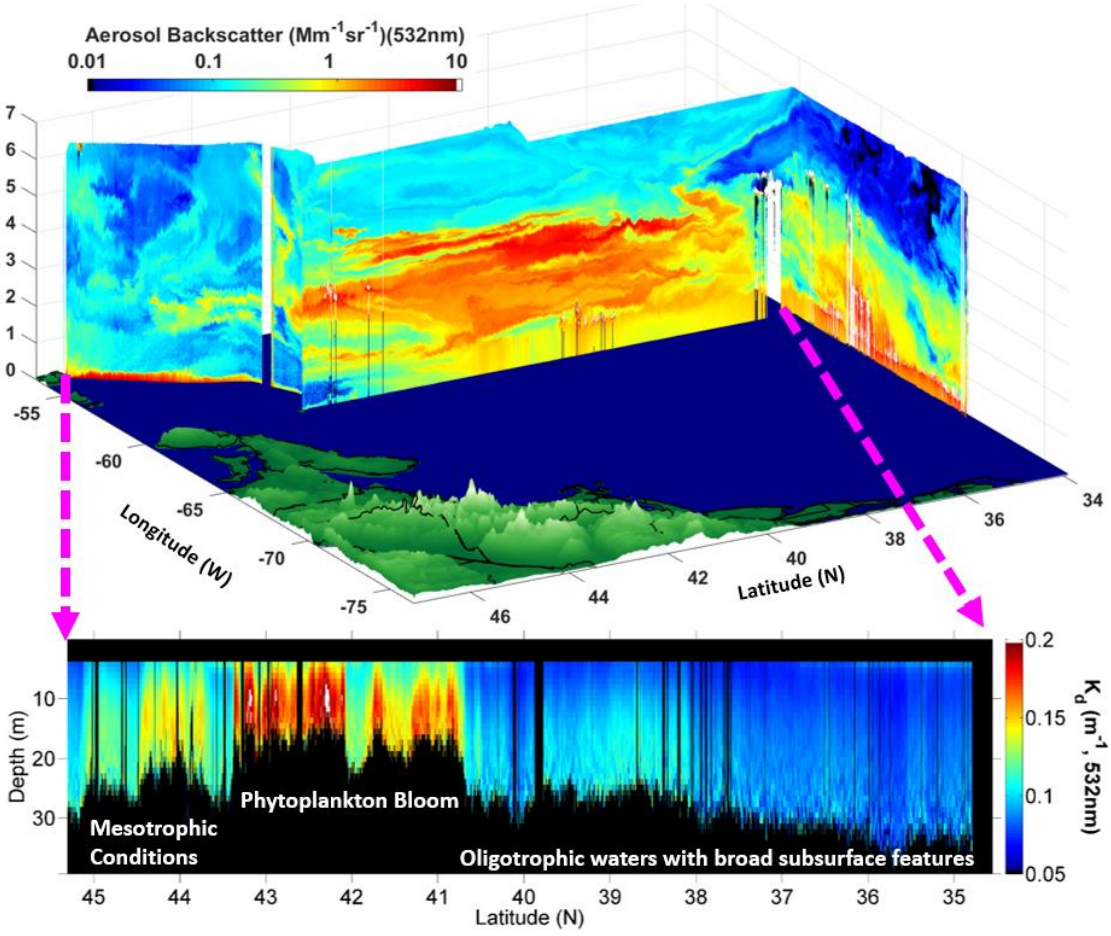

Figure 3. Along-track 'curtain' plots acquired with the NASA airborne HSRL-1 instrument on the May 2016 during a NAAMES deployment. (top panel) Vertically resolved aerosol backscatter in the atmosphere along the flight track in the North Atlantic. Vertical scale is in kilometers. (bottom panel) Vertically resolved diffuse attenuation coefficients in the ocean along the flight segment delineated by dashed pink arrows. Vertical scale is in meters. From 35° N to ~40° N, the transect sampled oligotrophic conditions with significant subsurface features north of 38° N. A strong near-surface bloom was encountered between ~41° N and ~43° N, followed by more mesotrophic waters with significant subsurface biomass between ~10 and 20 m depth.

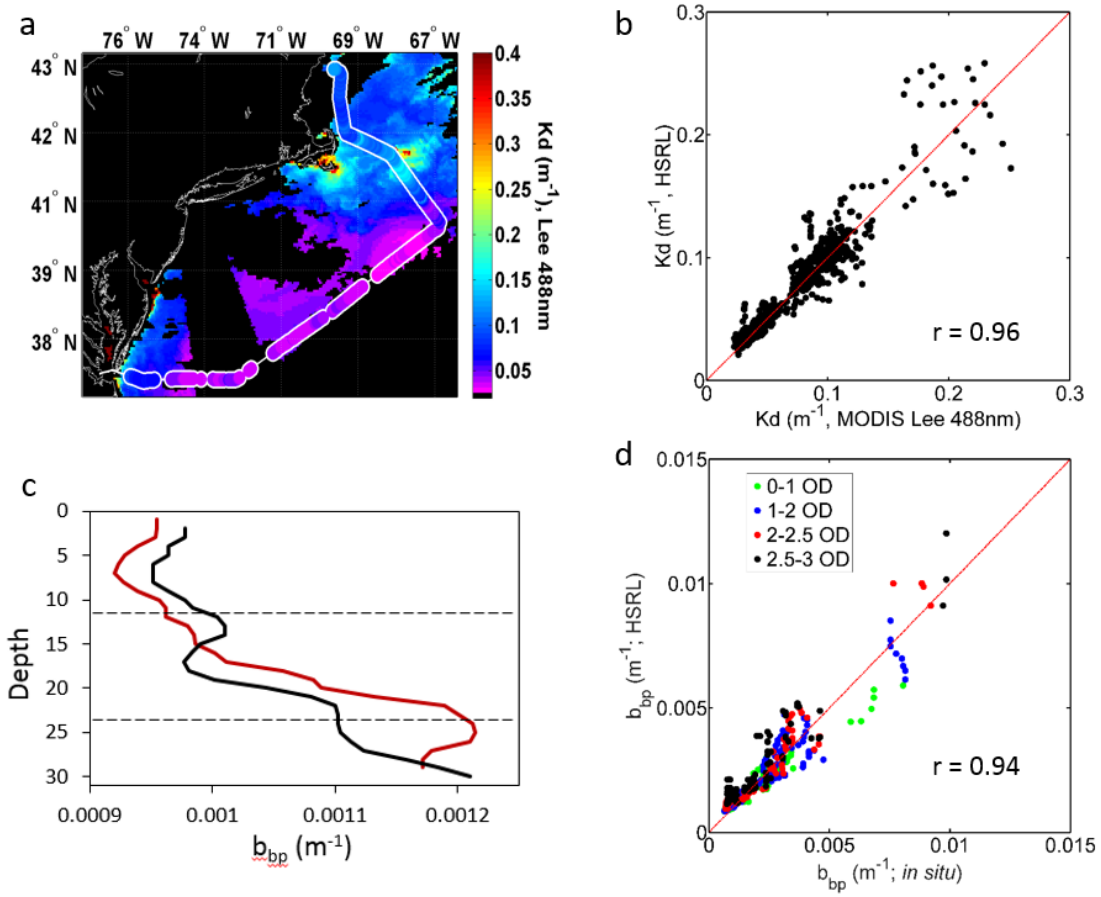

Figure 4. Results from the SABOR field campaign, which encompassed 24 flights with the HSRL-1 and 23 ocean sampling stations on the RV Endeavor. (a) MODIS K_d at 488 nm values (Lee et al. 2005) for July 18, 2014 (background color) and K_d retrieved with the HSRL-1 along a flight track on the same day (white outlined data; modified from Hair et al., 2016). HSRL-1 K_d values were calculated at 10 m depth and converted to 488 nm by accounting for the difference in pure seawater absorption. (b) K_d matchup data from HSRL-1 and MODIS for all flights during the SABOR campaign (modified from Hair et al., 2016). (c) Comparison of b_{bp} profiles from HSRL-1 (532 nm, red line) and in situ measurements (529 nm, black line) from a Wet Labs ECO BB3 instrument (modified from Schulien et al., 2017). (d) Matchup comparison of HSRL-1 and in situ b_{bp} data from the 16 offshore SABOR stations where overboard optical casts had near-coincident HSRL measurements (modified from Schulien et al., 2017). Colors indicate the optical depth of each sample.

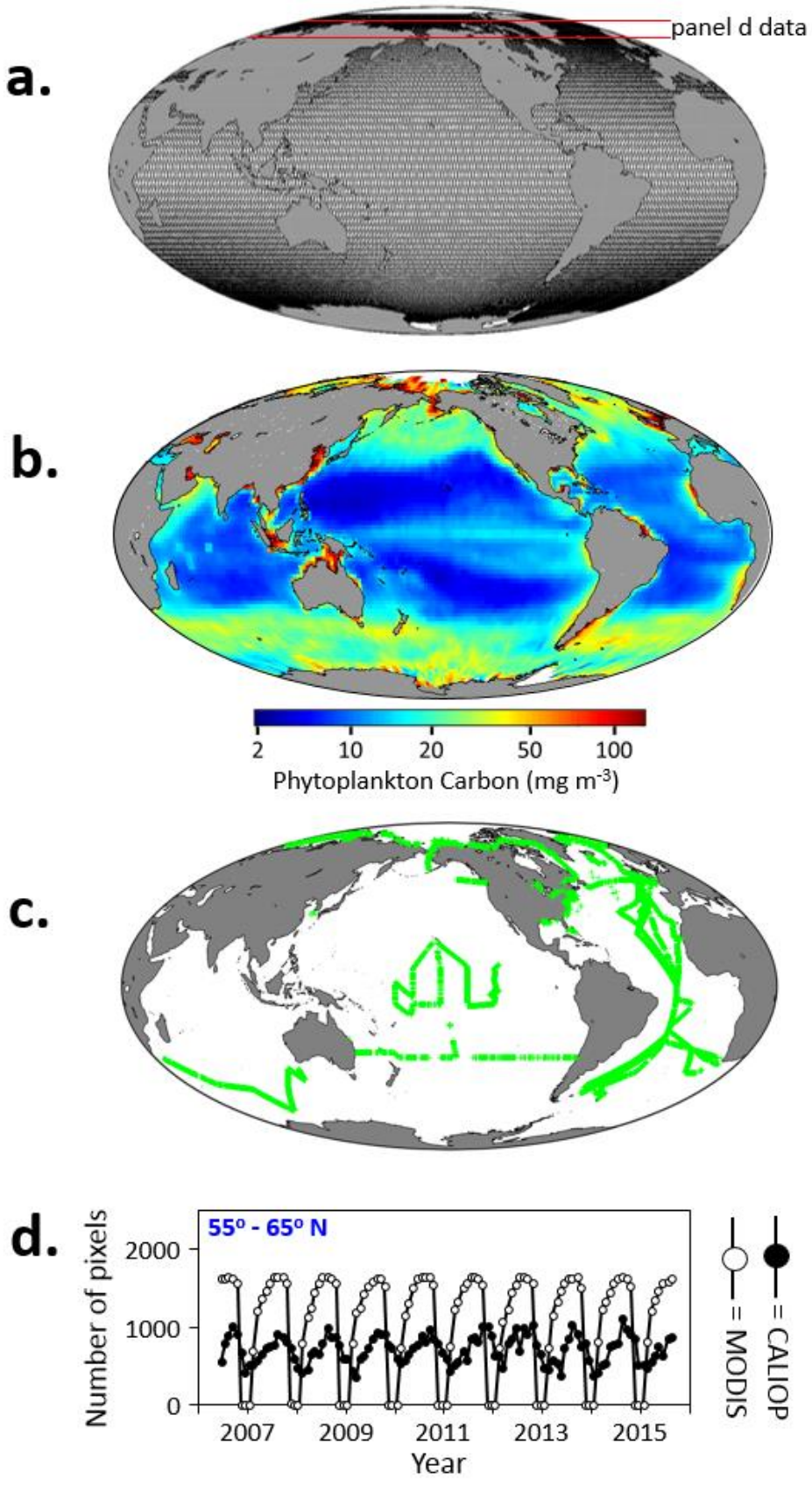
a.
panel d data
b.
2
10
20
50
100
Phytoplankton Carbon (mg m-3)
c.
d.
55º - 65º N
Number of pixels
2000
1000
0
2007
2009
2011
2013
2015
Year
= MODIS
= CALIOP

Figure 5.

Figure 5. Sampling of the global ocean with CALIOP. (a) CALIOP ground tracks achieved within a single 16-day repeat cycle. Red lines = 55° to 65° North latitude section used to compare CALIOP and MODIS data coverage in panel d. (b) CALIOP-based climatological annual average phytoplankton biomass (C_{phyto}) for the 2006 to 2012 period reported by Behrenfeld et al. (2013). (c) Location of all field b_{bp} data in the NASA SeaBASS data archive. These data required 13 years to collect, yet still leave most of the ocean unsampled in space and time. By comparison, CALIOP can provide an unbiased global sampling of b_{bp} every 16 days that can be used for global ocean science investigations and to refine algorithms for passive ocean color retrievals. (d) Comparison of CALIOP and MODIS pixel coverage per month for the 55° to 65° North latitude section identified in panel a (from Behrenfeld et al. 2016). Filled and unfilled symbols = Total number of 1° latitude × 1° longitude ice-free ocean pixels per month with valid CALIOP and MODIS b_{bp} data, respectively.

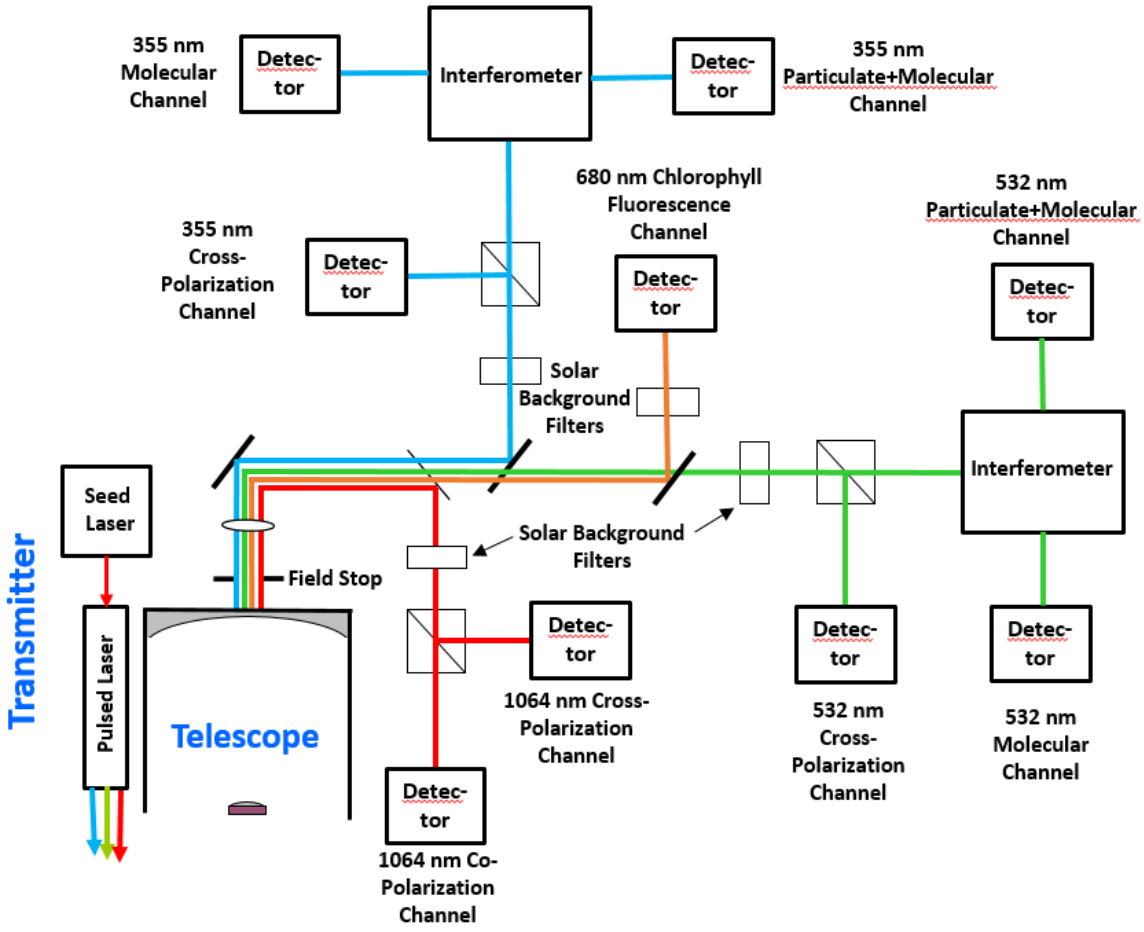

Figure 6. Simplified block diagram of primary components in the advanced spaceborne ocean-atmosphere optimized lidar discussed in Sections 6 and 7.

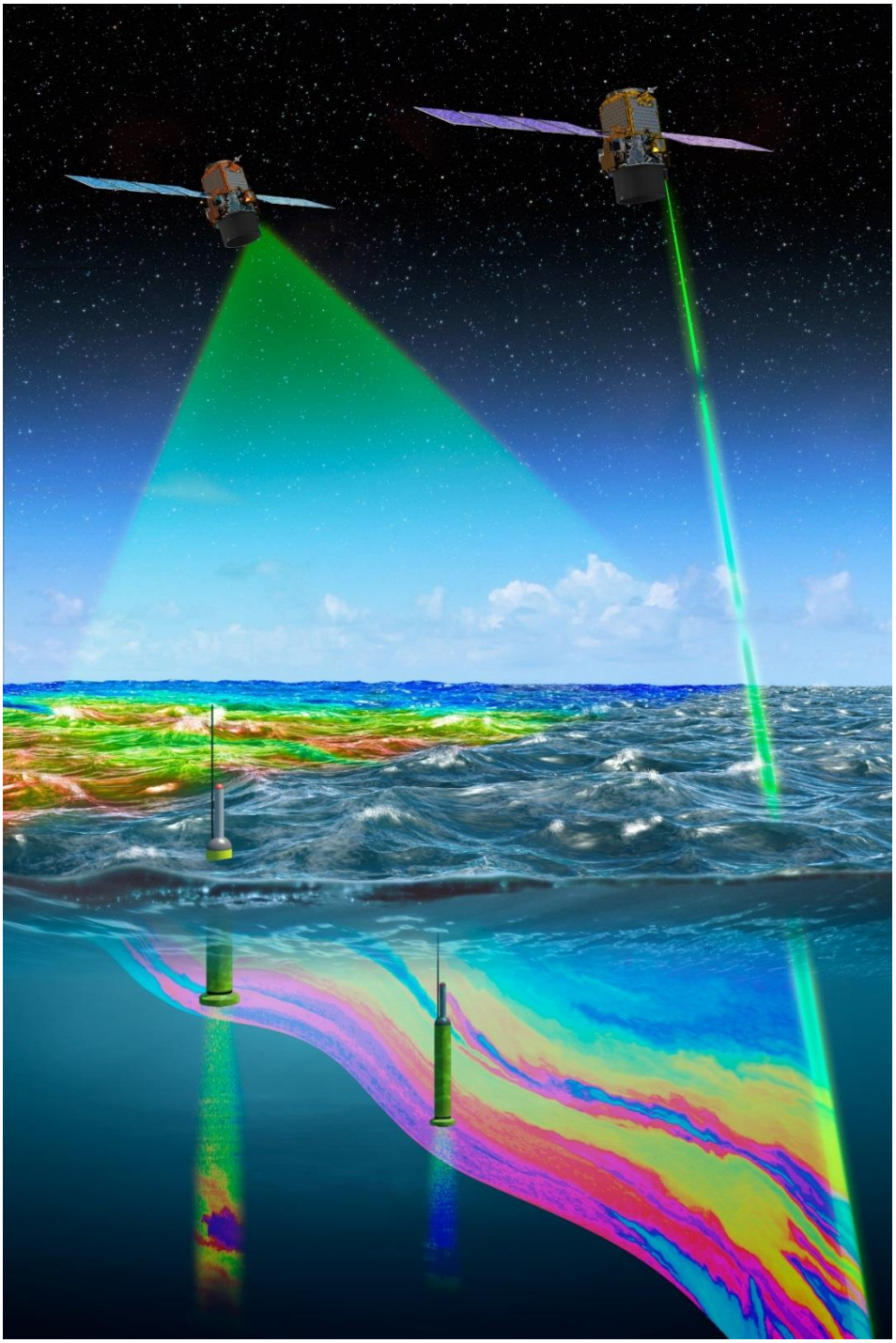

Figure 7. Artistic rendering of a virtual ocean observing constellation including complementary HSRL, ocean color, and polarimeter instruments supplemented by in situ Bio-Geo-Argo floats that extend the depth-resolving capability of the lidar.

FIGURE CAPTIONS

Figure 1. Illustration of the lidar time-of-flight ranging technique. (a)The laser transmits a short (e.g., 15 ns) pulse of laser light which is directed downward. (b) As the laser pulse travels toward Earth, photons are scattered from air molecules and cloud/aerosol particles in the atmosphere. (c) Shortly thereafter, the pulse penetrates the ocean where photons are also scattered by water molecules and suspended particles. Some of the scattered photons in the atmosphere and ocean are intercepted by the telescope, and the magnitude of this signal is recorded as a function of time by detectors located in the receiver. (d) Using the speed of light, time is converted to distance, creating a vertically-resolved profile of received backscatter.

Figure 2. The HSRL technique **(Box 1)** relies on the spectral separation between 180˚ backscatter from seawater and suspended particles (e.g., phytoplankton). The spectrum of particulate backscatter is nearly identical to that of the transmitted single-frequency laser pulse. Molecular backscatter, on the other hand, is shifted (~7.5 GHz at 532 nm) and broadened by Brillouin scattering processes (Hickman et al. 1991).

Figure 3. Along-track 'curtain' plots acquired with the NASA airborne HSRL-1 instrument on the May 2016 during a NAAMES deployment. (top panel) Vertically resolved aerosol backscatter in the atmosphere along the flight track in the North Atlantic. Vertical scale is in kilometers. (bottom panel) Vertically resolved diffuse attenuation coefficients in the ocean along the flight segment delineated by dashed pink arrows. Vertical scale is in meters. From 35^{o} N to ~40^{o} N, the transect sampled oligotrophic conditions with significant subsurface features north of 38^{o} N. A strong

near-surface bloom was encountered between ~41° N and ~43° N, followed by more mesotrophic waters with significant subsurface biomass between ~10 and 20 m depth.

Figure 4. Results from the SABOR field campaign, which encompassed 24 flights with the HSRL-1 and 23 ocean sampling stations on the RV Endeavor. (a) MODIS K_d at 488 nm values (Lee et al. 2005) for July 18, 2014 (background color) and K_d retrieved with the HSRL-1 along a flight track on the same day (white outlined data; modified from Hair et al., 2016). HSRL-1 K_d values were calculated at 10 m depth and converted to 488 nm by accounting for the difference in pure seawater absorption. (b) K_d matchup data from HSRL-1 and MODIS for all flights during the SABOR campaign (modified from Hair et al., 2016). (c) Comparison of b_{bp} profiles from HSRL-1 (532 nm, red line) and in situ measurements (529 nm, black line) from a Wet Labs ECO BB3 instrument (modified from Schulien et al., 2017). (d) Matchup comparison of HSRL-1 and in situ b_{bp} data from the 16 offshore SABOR stations where overboard optical casts had near-coincident HSRL measurements (modified from Schulien et al., 2017). Colors indicate the optical depth of each sample.

Figure 5. Sampling of the global ocean with CALIOP. (a) CALIOP ground tracks achieved within a single 16-day repeat cycle. Red lines = 55° to 65° North latitude section used to compare CALIOP and MODIS data coverage in panel d. (b) CALIOP-based climatological annual average phytoplankton biomass (C_{phyto}) for the 2006 to 2012 period reported by Behrenfeld et al. (2013). (c) Location of all field b_{bp} data in the NASA SeaBASS data archive. These data required 13 years to collect, yet still leave most of the ocean unsampled in space and time. By comparison, CALIOP can provide an unbiased global sampling of b_{bp} every 16 days that can be used for global ocean science investigations and to refine algorithms for passive ocean color retrievals. (d)

Comparison of CALIOP and MODIS pixel coverage per month for the 55^{o} to 65^{o} North latitude section identified in panel a (from Behrenfeld et al. 2016). Filled and unfilled symbols = Total number of 1^{o} latitude × 1^{o} longitude ice-free ocean pixels per month with valid CALIOP and MODIS b_{bp} data, respectively.

Figure 6. Simplified block diagram of primary components in the advanced spaceborne ocean-atmosphere optimized lidar discussed in Sections 6 and 7.

Figure 7. Artistic rendering of a virtual ocean observing constellation including complementary HSRL, ocean color, and polarimeter instruments supplemented by in situ Bio-Geo-Argo floats that extend the depth-resolving capability of the lidar.